The AMPK-v-ATPase-pH axis: a key regulator of the pro-fibrogenic phenotype of human hepatic stellate cells.

Giusi Marrone[1], Francesco De Chiara[2], Katrin Böttcher[1], Ana Levi[1], Dipok Dhar[1], Lisa Longato[1], Giuseppe Mazza[1], Zhenzhen Zhang[1], Martina Marrali[1], Anabel Fernández-Iglesias[3], Andrew Hall[7],Tu Vinh Luong[7], Benoit Viollet[4,5,6], Massimo Pinzani[1], Krista Rombouts[1]

1. Regenerative Medicine & Fibrosis Group, Institute for Liver & Digestive Health, University College London, Royal Free Hospital, London, UK
2. Liver Failure Group, Institute for Liver & Digestive Health, University College of London, Royal Free Hospital, London, UK
3. Liver Vascular Biology Research Group, Barcelona Hepatic Hemodynamic Laboratory, IDIBAPS Biomedical Research Institute – CIBEREHD, Barcelona, Spain
4. INSERM, Institut Cochin, Paris, France
5. CNRS UMR 8104, Paris, France
6. Université Paris Descartes, Sorbonne Paris cité, Paris, France
7. Royal Free Hospital, Department of Cellular Pathology, London, UK

Keywords: Vacuolar adenosine tri-phosphatase (v-ATPase), pH, human Hepatic Stellate Cells (HSC), liver fibrosis, AMP-activated protein kinase (AMPK), anti-fibrotic therapy.

Corresponding author: Giusi Marrone, Ph.D., current address: Institut d'investigacions Biomèdiques August Pi i Sunyer, Liver Vascular Biology Research Group, Barcelona Hepatic Hemodynamic Laboratory, Carrer del Rosselló, 149, 08036 Barcelona, Spain. Tel: +34932275400 ext 2971, email: MARRONE@clinic.cat

Corresponding author: Krista Rombouts, Ph.D. University College London - Institute for Liver and Digestive Health, Regenerative Medicine & Fibrosis Group, Royal Free Hospital. Rowland Hill Street, London, NW3 2PF, UK. Tel: +4402074332852, email: k.rombouts@ucl.ac.uk.

List of Abbreviations:

HSC Hepatic stellate cell

pHi Intracellular pH

pHe Extracellular pH

AMPK AMP-activated protein kinase

v-ATPase Vacuolar adenosine tri-phosphatase

ATP6V1A Vacuolar adenosine tri-phosphatase catalytic V1A subunit

ATP6V1B2 Vacuolar adenosine tri-phosphatase regulatory V1B2 subunit

ATP6V1C Vacuolar adenosine tri-phosphatase assembly V1C subunit

ATP6v0c Vacuolar adenosine tri-phosphatase transmembrane-proton-extrusion v0c subunit

BrdU 5-bromo-2-deoxyuridine

MTS 3-(4,5-dimethylthiazol-2-yl)-5-(3-carboxymethoxyphenyl)-2-(4-sulfophenyl)-2H-tetrazolium inner salt

qPCR quantitative polymerase chain reaction

MEF mouse embryo fibroblasts

BDL Bile Duct Ligation

H^+ proton

AMPKα1 AMP-activated protein kinase subunit α1

AMPKα2 AMP-activated protein kinase subunit α2

ATP Adenosine tri-phosphate

N Normal

CH Cirrhotic

CM Complete medium

SFM Serum free medium

p-AMPK phosphorylated AMPK

ACC Acetyl-CoA carboxylase

p-ACC phosphorylated acetyl-CoA carboxylase

AMPKα1-null AMP-activated protein kinase subunit α1 - deficient

AMPKα2-null AMP-activated protein kinase subunit α2 - deficient

AMPKα1α2-null AMP-activated protein kinase subunit α1α2 - deficient

Bafi Bafilomycin A1

KM KM91104

Diflu Diflunisal

A76 A769662

ZLN ZLN 024 hydrochloride

siRNA small interfering RNA

siC small interfering RNA negative control

siAMPKα1 AMPKα1-specific siRNA

PDGF-BB Platelet Derived Growth Factor BB

TGFβ1 Transforming Growth Factor β1

α-SMA alpha smooth muscle actin

Contributors: GM experimental design, data analysis, drafting of the manuscript; FDC, AH, TVL immunohistochemistry analysis; FDC, MM immunoblotting; KB, ZZ hepatic stellate cell culture; KB MEF culture; ZZ, AL performed qPCR of BDL liver samples; DD and LL provided BDL liver sample; BV provided MEFs; GM provided tissue; AFI provided HSC freshly isolated from human cirrhotic and healthy livers. MP critical review of the manuscript; KR isolation of primary hHSC, study concept and design, conceptual and intellectual input, critical review of the manuscript. All authors read and approved the final manuscript.

Financial Support: Giusi Marrone received a Sheila Sherlock Postdoctoral Fellowship from the European Association for the Study of the Liver. This work was supported by grants from the NIHR UCLH BRC and the Royal Free Charity (MP) and Innovate UK (KR).

Acknowledgment: We would like to thank Fred Gorelick Department of Medicine, Yale University School of Medicine, New Haven, Connecticut, USA for stimulating discussions and helpful suggestions.

Conflict of interest: The authors who have taken part in this study declared that they do not have anything to disclose regarding funding or conflict of interest with respect to this manuscript.

ABSTRACT

Liver fibrosis and cirrhosis are characterized by activation of hepatic stellate cells (HSC) which is associated with higher intracellular pH (pHi). The vacuolar H^+ adenosine-tri-phosphatase (v-ATPase) multi-subunit complex is a key regulator of intracellular pH homeostasis. The present work was aimed at investigating the functional role of v-ATPase in primary human HSC (hHSC) activation and its modulation by specific AMPK subunits. Here, we demonstrated that the expression of different v-ATPase subunits was increased in *in vivo* and *in vitro* activated hHSC, compared to non-activated hHSC. Specific inhibition of v-ATPase with Bafilomycin and KM91104 induced a down-regulation of the HSC fibrogenic gene profile, which coincided with increased lysosomal pH, decreased pHi, activation of AMPK, reduced proliferation, and a lower metabolic activity. Similarly, pharmacological activation of AMPK by treatment with Diflunisal, A769662 and ZLN024, reduced the expression of v-ATPase subunits and pro-fibrogenic markers. V-ATPase expression was differently regulated by AMPKα1 and AMPKα2, as demonstrated in mouse embryo fibroblasts (MEF) specific deficient for AMPKα subunits.

In addition, the activation of v-ATPase in hHSC was shown to be AMPKα1 dependent. Accordingly, pharmacological activation of AMPK in AMPKα1-depleted hHSC prevented v-ATPase downregulation. Finally, we showed that v-ATPase expression was increased in fibrotic livers from Bile Duct Ligated mice and in human cirrhotic livers. *Conclusions.* The down-regulation of v-ATPase might represent a new promising target for the development of anti-fibrotic strategies.

INTRODUCTION

Hepatic stellate cells (HSC) are liver-specific pericytes playing a key role in hepatic fibrogenesis. Following chronic liver tissue damage, HSC acquire a pro-fibrogenic, contractile and proliferative myofibroblast-like phenotype (activated HSC), which is ultimately responsible for the fibrogenic progression of chronic liver diseases (1, 2). It is established that *in vitro* activated rat and human HSC are characterized by a significantly higher baseline intracellular pH (pHi), in comparison to non-activated, freshly isolated HSC, due to an increased proton (H^+) extrusion rate (3, 4). The possibility of modulating the pro-fibrogenic phenotype of HSC by acting on the machinery responsible for the increased pHi, has been repeatedly suggested but not confirmed. One of the most recently characterized systems involved in the maintenance of pHi is the vacuolar adenosine tri-phosphatase (v-ATPase). This hetero-multimeric enzyme complex is composed of at least 14 different independent subunits assembled to a cytosolic ATP-hydrolytic domain (V_1) and a membrane-bound proton-translocating domain (V_0) docked on/in the membrane. V-ATPase is located both in endomembrane systems and in the plasma membrane and is therefore able to maintain pHi by actively transporting protons from the cytoplasm to the lumen of intracellular compartments i.e. lysosomes, as well as from the cytoplasm to the plasma membrane i.e. into the extracellular space (5). Recent experimental evidence in the kidney suggests that v-ATPase is regulated by the energy-sensing enzyme AMP-activated protein kinase (AMPK) (6, 7). AMPK is a heterotrimeric serine/threonine kinase consisting of three subunits α, β and γ, each expressed in different isoforms as the result of distinct gene codifications. AMPKα1 is widely expressed across tissues, and is predominantly

localized in the cytosol whereas AMPKα2 is more restricted in its tissue-and intracellular distribution (8, 9). Both AMPKα isoforms are expressed in human liver tissue (10). Previous studies showed that AMPK activation is characterized by phosphorylation of the threonine residue (Thr-172) in the activation loop of AMPKα1 and AMPKα2. Once activated, AMPK stimulates ATP-generating catabolic pathways and inhibits energy-consuming processes (9). Activation of AMPK has also been shown to interfere with the pro-fibrogenic HSC phenotype by inhibiting PDGF-BB-induced cell proliferation and TGF-β-induced fibrogenic responses (11-13) suggesting that agents able to promote AMPK activation could be employed as anti-fibrotic agents.

Until now, no information is available regarding the expression and distribution of v-ATPase in human HSC, and more precisely whether it is regulated by AMPK and *vice versa*, whether v-ATPase activation can affect AMPK function. Accordingly, the present study was designed to evaluate the expression and functional role of 4 different v-ATPase subunits (V1A, catalytic; V1B2, regulatory; V1C, assembly; v0c, transmembrane-proton-extrusion) in hHSC isolated from cirrhotic liver (*in vivo* activated HSC) and in *in vitro* activated primary hHSC. We assessed whether changing pHi by v-ATPase inhibition could affect hHSC activation and whether v-ATPase expression and activity can be modulated by specific AMPKα subunits. Finally, we evaluated whether the pharmacological activation of AMPK is able to affect v-ATPase activity. In order to provide translational information, the expression of v-ATPase was investigated in human liver tissue obtained from healthy and cirrhotic subjects and by employing the bile duct ligation (BDL) animal model of liver fibrosis.

Our results indicate that an increased v-ATPase expression is a key feature of activated hHSC as well as of liver tissue characterised by active fibrogenesis. V-ATPase inhibition is able to induce a net down-regulation of hHSC pro-fibrogenic phenotype whereas pharmacological activation of AMPK decreases v-ATPase expression and prevents extracellular acidification by hHSC in an AMPKα1-dependent manner.

MATERIALS AND METHODS

A complete description of materials and methods can be found in the online supplementary material.

Cell cultures

Isolation and culture of human hepatic stellate cells (hHSC)

Cells were isolated from wedge sections of human liver obtained from patients undergoing liver resections at the Royal Free Hospital after giving informed consent (EC01.14-RF). Cell isolation was performed according to a published protocol (14), with modifications for human liver (15).

Treatments

Primary human HSC were cultured in 20% serum enriched medium for 24 hours followed by incubation in serum free medium (SFM) for 24h before each experimental treatment to avoid interference with growth factors and amino acids enriched in foetal bovine serum (16-18). Data obtained from cells cultured in complete medium (CM) are reported in figure legends. Specific treatment with v-ATPase inhibitors, Bafilomycin A1

and KM91104, with AMPK activators, Diflunisal, A769662 and ZLN 024 hydrochloride, and with TGFβ1 and PDGF-BB are described in the online supplementary methods.

Intracellular ATP

hHSC were seeded at a density of 10000 cells/well/100uL in a 96-well plate in CM and serum-starved for 24h followed by incubation with the v-ATPase inhibitors for 48h. Cell lysis was induced using the CellTiter-Glo® Reagent (Promega), according to the manufacturer's specification. Luminescence was recorded and the intracellular ATP concentration was calculated from an ATP standard curve and normalized to hHSC proliferation.

Animal models of liver cirrhosis

Male, Balb/c mice were obtained from the comparative biological unit at the Royal Free and University College Medical School (Royal Free Campus, London, UK). All animals were given free access to normal rodent chow (expanded SDSRM 1; Special Diet Services, Witham, UK) and water. BDL or a sham operation was performed as described previously (19). Experiments were terminated after 14 days and liver tissue was snap frozen and stored at −80°C until further analysis.

Statistical analysis

In vitro experiments were carried out with a minimum of three independent cell preparations and at least three experimental replicates. Results are expressed as mean values ± SEM and compared using one-way analysis of variance followed by Dunnet's

or Tukey's multiple comparison post hoc tests or compared using a student t-test, where appropriate (GraphPad Prism; GraphPad,La Jolla, CA). P values of ≤0.05 were considered significant.

RESULTS

Increased expression of v-ATPase in in vivo and in vitro activated human HSC.

V-ATPase protein expression was evaluated in hHSC and compared between freshly isolated hHSC obtained from cirrhotic liver, i.e. *in vivo* activated cells, and from freshly isolated hHSC obtained from healthy liver. As shown in Figure 1A, the expression of the v-ATPase catalytic V1A, the regulatory V1B2 and the transmembrane-proton-extrusion v0c subunit showed to be upregulated in hHSC isolated from cirrhotic liver (CH) in comparison to hHSC obtained from normal, healthy liver (N), whereas the assembly subunit V1C was scarcely detectable. Furthermore, variations in v-ATPase protein expression during the process of *in vitro* hHSC activation was assessed from culture passage 1 to subsequent culture passage 4 and demonstrated a significant increase in protein expression for subunits V1A, V1C and v0c with a tendency to increase for the V1B2 subunit (Figure 1B).

In a next set of experiments, cells were treated for 24 hrs with PDGF-BB or TGFβ1 and v-ATPase subunit V0c mRNA expression showed a tendency to increase upon TGFβ1 stimulation, whereas at the protein level v-ATPase subunit V0c showed a tendency to be downregulated by PDGF-BB (Supplementary Figure 2) indicating possible post-translational modifications upon treatment with specific stimuli. Next, the total protein and the intracellular distribution was investigated as the activity of V-ATPases *in vivo* is

tightly regulated by reversible association and dissociation of the V1 and V0 domains, thus when functionally assembled V-ATPase is localized in intracellular compartments/membranes and in the plasma membrane (20). No significant changes were observed in total protein expression between cells cultured in complete serum rich medium (CM) and serum free medium (SFM) (Figure 1C). In contrast, subcellular protein fractionation analysis showed that hHSC cultured in CM, containing growth factors and amino acids, expressed all v-ATPase subunits predominantly at the membrane level (ME), whereas in serum starved hHSC the V1B2 subunit became more cytosolic (CE) (Figure 1D), suggesting an intracellular compartmentalization and dynamic translocation of v-ATPase subunits under different culture conditions.

To investigate the possible association between v-ATPase and AMPK in hHSC, we first investigated the expression of different AMPKα subunits in hHSC in serum rich and serum starved conditions. AMPKα1 mRNA expression was significantly up-regulated in SFM conditions in comparison to hHSC cultured in CM (Figure 1E), whereas no differences were observed at the protein level (Figure 1F), suggesting post-translational modifications. AMPKα2 protein expression was barely detectable in hHSC as was assessed by qRT-PCR (Figure 1E), western blot analysis (60ug), and immunofluorescence (Figure 1F).

Overall, these results indicate that v-ATPase is highly expressed in *in vivo* activated hHSC and the expression increases during *in vitro* culture activation. Moreover, AMPKα1, in contrast to AMPKα2, is strongly expressed in hHSC.

V-ATPase inhibition affects hHSC proliferation, metabolic activity and pro-fibrogenic phenotype.

To better define how v-ATPase activity affects hHSC activation, cells were treated for 48h with v-ATPase inhibitor Bafilomycin which inhibits specifically the v-ATPase proton pump (V-ATPase subunit ATP6V0C/V0) (21), and KM91104 which specifically targets the interaction between v-ATPase subunit a3 and subunit B2 (22). Upon treatment, cells exhibited a marked reduction in metabolic activity (Figure 2A), a dose-dependent decrease in cell proliferation (Figure 2B), and a dose-dependent increase in intracellular ATP levels (Figure 2C). Of note, Bafilomycin-induced v-ATPase inhibition coincided with a significant downregulation of the mRNA expression of HSC activation markers such as α-SMA (Figure 2D) and pro-collagen I (Figure 2E), while KM91104 was ineffective. These experiments clearly demonstrated that both inhibitors, due to their different mode of action, interfere differently with the regulation of different v-ATPase subunits.

V-ATPase regulates intracellular pH of hHSC.

Next, v-ATPase activity and inhibition was assessed to clarify the differences in the effects of the two v-ATPase inhibitors. KM91104-treated hHSC showed a reduced expression of all v-ATPase subunits (Figure 3A-D), while Bafilomycin-treated hHSC showed a significant down-regulation only of subunits V1C and v0c (Figure 3C-D). Next, the effect of both v-ATPase inhibitors was further assessed on pH homeostasis by employing a neutral red uptake assay. Serum starved hHSC displayed a higher neutral red uptake in comparison to cells cultured in CM reflecting a more acidic pH inside the intracellular compartments i.e. lysosomes and endosomes (Figure 3E). In contrast,

Bafilomycin-treatment (10nM) in serum free condition reversed this effect as demonstrated by a decreased uptake of neutral red when compared to control cells. Similar results, but less prominent, were obtained with KM91104 treatment (Figure 3E). Furthermore, changes in cytosolic pH were quantified by employing a fluorometric BCFL-AM assay. Treatment with 10nM Bafilomycin or 10nM KM91104 was followed by a significant decrease in cytosolic pH (Figure 3F). Since inhibition by Bafilomycin had a marked effect on hHSC pro-fibrogenic phenotype (Figure 2), pHi was measured following an acidic load with NH_4Cl. The pHi of both Bafilomycin-treated (1nM) and control cells increased rapidly over 8 minutes, i.e. steep slope (Figure 3G). In contrast, a less steep steady slope (<45.8%) was observed in 10nM Bafilomycin-treated hHSC, with a higher increase in baseline pHi after 1 minute of acidic load, in comparison to vehicle-treated cells (Figure 3G). Next, v-ATPase activity as proton pump at the plasma membrane was assessed by quantifying the pHe in all cell culture media, which showed to be more acidified in v-ATPase inhibitor-treated cells in comparison to vehicle-treated hHSC (Supplementary Table 1). Overall, these data suggest an important role for v-ATPase in pH homeostasis but also highlight the function of non-v-ATPase related pumps which become active to compensate the reduction/loss of v-ATPase activity following treatment with specific inhibitor. Next, the phosphorylation of AMPK at Thr172 was analyzed to further investigate whether inhibition of v-ATPase activity affects AMPK activity in hHSC. Bafilomycin treatment for 48h resulted in a marked increase in AMPK phosphorylation (Figure 3H). Taken together, these findings suggest that v-ATPase inhibition by different pharmacological inhibitors correlates with changes in pHi and pHe homeostasis in hHSC. Furthermore, v-ATPase inhibition by Bafilomycin, but not

KM91104, leads to activation/phosphorylation of AMPK and inhibition of hHSCs' pro-fibrogenic profile.

Pharmacological activation of AMPK downregulates v-ATPase expression in hHSC.

To investigate the role of the AMPK-v-ATPase-pH axis in hHSC, cells were treated with the AMPK allosteric, direct activators A769662 (23) and ZLN024 (24) both inhibiting dephosphorylation of p-AMPK, and Diflunisal, a salicylic acid derivative with analgesic and anti-inflammatory effects, which has been shown to act as a strong CBP/p300 inhibitor (25, 26). First, the effect of all activators was tested on hHSC metabolic activity and proliferation (Supplementary Fig. 1). Cells treated with Diflunisal (100uM) showed a significant decrease in metabolic activity and proliferation, without morphological changes indicative of cell death, whereas 1mM was clearly cytotoxic (Supplementary Fig. 1A-C). Treatment with A769662 showed no significant effect on metabolic activity and proliferation at the dose of 10uM whereas higher doses (100uM-200uM) were cytotoxic. Treatment with ZLN024 had no effect on hHSC metabolic activity and proliferation (Supplementary Fig. 1C-E). Next, AMPK activation was assessed by employing ELISA to quantify the phosphorylation of AMPK-Thr172 in hHSC treated with all AMPK activators under investigation. Treatment with 100uM of Diflunisal, 10μM A769662 and ZLN024 at all the concentrations employed resulted in increased AMPK phosphorylation of Thr172-AMPK (Figure 4A). Of all the AMPK activators tested, only Diflunisal treatment demonstrated a reduction in hHSC metabolic activity and proliferation (Supplementary Fig. 1A) which correlated with increased AMPK phosphorylation. Diflunisal further induced AMPKs' downstream target Acetyl-CoA-

Carboxylase (ACC) by phosphorylating Ser79 (Figure 4B). Of note, Diflunisal treatment induced a down-regulation of α-SMA (Figure 4C) and pro-collagen I (Figure 4D) as was previously shown for hHSC treated with the v-ATPase inhibitor Bafilomycin (Figure 2D and 2E). Importantly, activation of AMPK by Diflunisal and A769662, but not ZLN024, was associated with a decreased protein expression of all v-ATPase subunits (Figure 4E), and coincided with changes in v-ATPase activity as shown by a 51% and 38% reduction in extracellular H^+ concentration, respectively (Supplementary Table 2). These data demonstrate that the compounds tested have different modes of AMPK activation in hHSC. In addition, we show that both Diflunisal and A769662 reduced v-ATPase expression while ZLN024 had no effect. These data demonstrate that pharmacological activation of AMPK in hHSC is correlated with v-ATPase protein expression and activity.

V-ATPase expression is differentially regulated by AMPKα1 and AMPKα2 and AMPKα1 regulates v-ATPase in hHSC.

The data so far suggest that inhibition of v-ATPase activity leads to activation of AMPK and *vice versa* activation of AMPK reduces v-ATPase activity. Therefore, we further defined the role of different AMPK subunits on each v-ATPase expression/activation in well-characterized genetically modified MEF deficient for specific subunits i.e. AMPKα1, AMPKα2 and AMPKα1α2. First, the mRNA expression of all v-ATPase subunits was assessed in the different AMPKα deficient fibroblasts. The expression of all v-ATPase subunits was significantly higher in AMPKα2-null MEF in comparison to the other AMPKα deficient fibroblasts and Wild Type (WT) MEF (Figure 5A). AMPKα1α2-null MEF showed increased expression of all subunits, with V1C and v0c showing

significantly higher expression in comparison to WT MEF. AMPKα1-null MEF showed a significant increase in the regulatory subunit V1B2 and a strong decrease in the transmembrane-proton-extrusion v0c subunit compared to WT MEF. These data indicate that a deficiency in a specific AMPK subunit coincides with variations in v-ATPase subunits gene expression.

To further define whether the previously observed decrease in v-ATPase expression in Diflunisal and A769662-treated cells was AMPK-dependent (Figure 4), WT and AMPKα1α2-null MEF were treated with Diflunisal and A769662 for 24h. Diflunisal-treated WT MEF showed a significant decrease in protein expression in all four v-ATPase (Figure 5B) similar to Diflunisal-treated hHSC (Figure 4E), whereas in Diflunisal-treated AMPKα1α2-null MEF, this downregulation in V1A and V1B2 protein expression was abrogated indicating an AMPK-dependent effect (Figure 5B). On the other hand, a small but significant decrease in V1C and v0c expression was still observed in AMPKα1α2-null treated cells, indicating AMPK-independent effects (Figure 5B). In contrast to Diflunisal, A769662 treatment had a significant effect on V1C and v0c in WT cells and v0c expression in AMPKα1α2-null MEF but no effect on V1A and V1B2 subunits in both cell types under investigation.

Next, siRNA against AMPKα1 was employed to investigate whether the expression of v-ATPase was AMPKα1-dependent in hHSC (Figure 5C). SiRNA-depleted AMPKα1 hHSC were treated with Diflunisal and A769662 and v-ATPase protein expression was assessed. Interestingly, the previously observed Diflunisal and A769662-induced down-regulation of v-ATPase V1A, V1B2 and V1C expression (Figure 4E) was completely prevented in AMPKα1-silenced hHSC (SiC *vs* SiAMPKα1) (Figure 5D), while the down-

regulation of v0c expression was partially abrogated (Figure 5D). Furthermore, silencing of AMPKα1 expression in hHSC revealed that Diflunisal and A769662 pharmacological activation of AMPK in AMPKα1-depleted hHSC prevented v-ATPase downregulation except for v-ATPase V1A subunit.

V-ATPase expression is upregulated in vivo and in human liver cirrhosis.

In vivo activation of HSC is the result of the interaction with the surrounding cellular and molecular microenvironment undergoing sustained injury. Thus, we analyzed v-ATPase expression in a BDL mice model of liver fibrosis and in liver tissue obtained from healthy and cirrhotic patients. As shown in Figure 6A, a significant increase in mRNA levels of V1B2 and v0c was observed in BDL-induced animals, whereas no significant changes were observed for V1A and V1C subunits, in comparison to sham-control mice. This was further confirmed at the protein level (Figure 6B). Next, immunohistochemistry showed a co-localization of α-SMA positive hHSC with v-ATPase in the perisinusoidal space of Disse and all 4 v-ATPase subunits exhibited an increased expression and cellular distribution in punctuate/granular structures in human cirrhotic liver tissue (markedly enhanced in parenchymal cells), in comparison to healthy liver, as shown in Figure 6C. Taken together, these results indicated that v-ATPase is increased in fibrotic mouse tissue and in human cirrhotic livers, corroborating its implication in the initiation and progression of the fibrogenic process occurring in chronic liver diseases.

DISCUSSION

Hepatic stellate cells (HSC) are the main cellular effectors of liver fibrogenesis (1, 2). To date, no anti-fibrotic therapies for chronic liver disease have been introduced in clinical practice (27-29). V-ATPase are large multi-subunit complexes (V_1V_0) and are ATP-dependent proton (H^+) pumps which regulate pH homeostasis by pumping H^+ against their electrochemical gradient. Thus, v-ATPase acidifies intracellular compartments by pumping in H^+ into lysosomes and by pumping out H^+ across the plasma membrane into the extracellular space (30). We hypothesized that the higher baseline intracellular pH found in activated HSC may originate not only from the activity of the Na^+/H^+ exchanger (3, 4) but also from v-ATPase expression and activity. We found that all 4 v-ATPase subunits under investigation were highly expressed in fibrotic tissue of mice and cirrhotic human livers, as well as in hHSC activated both *in vitro* and *in vivo*. Moreover, intracellular v-ATPase was localized in intracellular compartments and on the plasma membrane depending on different culture conditions. These observations led to the hypothesis that v-ATPase could play an important role in regulating H^+ fluxes throughout the cell upon changes in the microenvironment like those occurring in conditions of chronic liver tissue damage and progressive fibrogenesis (31).

The pioneer studies of Di Sario and colleagues demonstrated the importance of the Na^+/H^+ exchanger in pHi regulation in HSC (4). With the present work we have demonstrated for the first time a key role for v-ATPase and its association with AMPK in regulating pHi in primary human HSC (Figure 7). Bafilomycin-induced inhibition of v-ATPase led to AMPK phosphorylation, which correlated with a significant reduction in hHSC pro-fibrogenic profile. This observation is in agreement with data demonstrating that Bafilomycin-treated murine HSC did not acquire a myofibroblast-like phenotype as

a consequence of a decreased autophagic flux (32). In our study, the down-regulation of pro-collagen I and α-SMA was observed after treatment with Bafilomycin but not with KM91104. This could be explained by the fact that Bafilomycin and KM91104 inhibit v-ATPase with different modalities. Bafilomycin acts by inhibiting proton flow through the v-ATPase pump (21), although after 48 hours of treatment an acute acid load is still able to induce an increment in pH. This suggests that other pumps, such as the Na^+/H^+ exchanger, are still active and exert a compensatory effect for the lack of active v-ATPase (3, 33, 34). In contrast, KM91104 is a weaker inhibitor than Bafilomycin since it specifically targets the interaction between V-ATPase subunits a3 and B2 (22), without interfering with the pump activity

To investigate the role of the AMPK-v-ATPase-pH axis in hHSC we demonstrated that primary hHSC express predominantly AMPKα1 whereas AMPKα2 is scarcely detectable (Figure 1E and 1F) and genetically modified AMPKα1/α2 MEF (23) showed a clear association between different v-ATPase subunits and specific AMPKα subunits. Furthermore, cells were treated with the AMPK allosteric, direct activators A769662 (23) and ZLN024 (24) both known to inhibit dephosphorylation of p-AMPK, and Diflunisal, a salicylic acid derivative with analgesic and anti-inflammatory effects, which has shown to be a strong CBP/p300 inhibitor (25, 26), and very recently demonstrated to be key in activation of hHSC (35). We demonstrate that both Diflunisal and A769662 reduce v-ATPase expression while ZLN024 had no effect. In addition, Diflunisal downregulates hHSC activation markers similarly as observed in hHSC treated with v-ATPase inhibitor Bafilomycin. These results are in line with a recent study demonstrating different working mechanisms through which salicylihalamide A and Bafilomycin inhibit v-ATPase

(25) as some effects of salicylate-based drugs, particularly on cellular metabolism, are mediated by AMPK (26). Importantly, our study demonstrates for the first time that Diflunisal acts as an AMPK activator in hHSC. Furthermore, Diflunisal-induced down-regulation in specific v-ATPase subunits expression was completely prevented in MEF deficient of AMPKα1α2, further corroborating the correlation between v-ATPase and AMPK. These findings were further explored in hHSC silenced for AMPKα1 and revealed that siRNA against AMPKα1 abrogates the downregulation in v-ATPase and that Diflunisal and A769662 exert their effect specifically on v-ATPase. Moreover, the importance of v-ATPase was further shown in an *in vivo* model of fibrosis and in human liver tissues demonstrating a co-localization of α-SMA positive cells with v-ATPase subunits and demonstrated an increased expression of v-ATPase in diseased liver. In conclusion, this study demonstrates that pharmacological inhibition of v-ATPase via AMPKα1 leads to an inhibition of the pro-fibrogenic hHSC phenotype. Accordingly, our results provide a solid platform for the design of drugs acting on the AMPK-v-ATPase-pH axis as potential new strategies for the treatment of liver fibrosis.

FIGURES LEGENDS

Figure 1: **Increased expression of v-ATPase in *in vivo* and *in vitro* activated human HSC.** (A) Representative western blots with histograms of v-ATPase subunits V1A, V1B2, V1C, v0c in hHSC isolated from human cirrhotic (CH) and normal (N) tissues, (B) in *in vitro* activated hHSC passage 1 (p1) to passage 4 (p4). (C) V-ATPase protein expression in total cell lysates and (D) in subcellular compartments of hHSC (CE,

cytosolic; ME, membrane; NE, nuclear) cultured in complete medium (CM) or serum free medium (SFM). n=3 per condition; *p<0.05 vs. Normal and p1. (E) Relative mRNA expression of AMPKα1 and AMPKα2 in hHSC cultured in CM and SFM. n=3 per condition; *p<0.05 vs. CM. (F) Representative western blot and fluorescence images of AMPKα1 and AMPKα2 in hHSC cultured in CM or SFM. n=2 per condition.

Figure 2: **Effects of V-ATPase inhibition on hHSC phenotype *in vitro*.** (A) Concentration-dependent regulation of cell metabolism (MTS), (B) DNA synthesis (BrdU), (C) intracellular ATP levels (Luminescence), and (D) α-SMA and (E) pro-collagen I mRNA expression in hHSC incubated for 48h with v-ATPase inhibitors Bafilomycin A1 and KM91104 (1nM, 10nM), or vehicle (veh, DMSO). n=4 per condition; *p<0.05 vs. veh (A-C). n=3 per condition; ***p<0.05 vs. veh (D-E).

Figure 3: **Effects of V-ATPase inhibition on v-ATPase expression and activity in hHSC.** Representative western blot with histogram of v-ATPase subunit V1A (A), V1B2 (B), V1C (C) and v0c mRNA expression (D) in hHSC incubated for 48h with either vehicle (veh, DMSO) or 1nM and 10nM of Bafilomycin A1 and KM91104. n=3 per condition; *p<0.05 vs. veh. (E) Representative images of neutral red staining (20x) and quantification in hHSC cultured in complete medium (CM) or serum free medium (SFM) and treated as described in A-D. n=4 per condition; *p<0.05 vs. veh. (F) Fluorescent quantification of BCFL-AM after a standard load protocol and (G) after an acidic load procedure in hHSC previously treated for 48h with (1-10nM) KM91104 and/or Bafilomycin A1 (1-10nM) , or its vehicle. n=4 per condition; *p<0.05 vs. veh. (H) Representative western blot and histogram of P-AMPK(Thr172) normalized to total AMPKα in hHSC treated with v-ATPase inhibitors. n=3 per condition; *p<0.05 vs. veh.

Figure 4: **Effects of AMPK activation on v-ATPase expression and pro-fibrogenic profile in hHSC.** AMPK activation evaluated by ELISA (A) and western blot (B) in hHSC 24h treated with Diflunisal (A-B) or AMPK activators A769662 and ZLN 024 hydrochloride (A). n=3 per condition; *p<0.05 vs. veh. Relative α-SMA (C) and pro-collagen I mRNA expression (D) in hHSC treated with Diflunisal (10nM-100uM) for 24h or vehicle. n=3 per condition; *p<0.05 vs. veh. (E) Representative Western blot with histogram of v-ATPase subunits normalized to α-Tubulin in hHSC after 24h of incubation with 100uM Diflunisal, 10uM A76, 100uM ZLN or its vehicle (DMSO). n=3 per condition; *p<0.05 vs. veh.

Figure 5: **V-ATPase expression is differentially regulated by AMPKα1 and AMPKα2 and AMPKα1 regulates v-ATPase in hHSC.** (A) Relative mRNA expression of v-ATPase subunits V1A, V1B2, V1C and v0c in AMPKα1-null, AMPKα2-null, AMPKα1α2-null and wild type (WT) MEF. n=3 per group; *p<0.05 vs. corresponding values of WT. (B) Representative western blot with histogram of v-ATPase subunits from wild-type (WT) or AMPKα1α2-null MEF after incubation with 100uM Diflunisal (Diflu), 10uM A769662 (A76) or its vehicle (Veh) for 24h. n=3 per group; *p<0.05 vs. corresponding vehicle. (C) Representative western blot of AMPKα1 with histogram of the corresponding protein in SiRNA-AMPKα1 silenced hHSC. n=4 per condition; *p<0.05 versus scrambled control (siC). (D) Representative western blot with histograms of v-ATPase subunits on lysates from AMPKα1-siRNA depleted hHSC treated with 100uM Diflunisal (Diflu) and 10uM A769662 (A76), n=3 per group; *p<0.05 vs. corresponding vehicle; **p<0.05 vs. all corresponding values (v0c).

Figure 6: **v-ATPase expression in BDL mice and liver human tissues.** (A) Hepatic mRNA expression and (B) protein levels of v-ATPase subunits in cirrhotic mice. n=5 per group; *p<0.05 vs. corresponding sham. (C) Representative images of immunohistochemistry of α-SMA co-localization with v-ATPase subunits in normal (N) and cirrhotic (CH) human liver tissues, and immunohistochemistry of v-ATPase subunits in normal (N) and cirrhotic (CH) human liver tissues (x100).

Figure 7: **V-ATPase-AMPK-pH regulation in human HSC.** In vivo and *in vitro* activated human HSC demonstrate an increased expression of v-ATPase. Pharmacological inhibition of v-ATPase reduced hHSC proliferation, metabolic activity and pro-fibrogenic profile through changing intracellular pH (pHi). Pharmacological activation of AMPK downregulates v-ATPase expression and AMPKα1 regulates v-ATPase in hHSC.

Supplementary Figures Legend

Supplementary Fig. 1: (A, D) Concentration-dependent regulation of cell metabolism (MTS) and (B, E) DNA synthesis (BrdU) in hHSC after 24h of incubation with either Diflunisal (A-B) or AMPK activators A769662 and ZLN 024 hydrochloride (D-E). n=4 per condition; *p<0.05 vs. veh. (C) Representative images of cell phenotype after treatment indicated.

Supplementary Fig. 2: (A) Relative mRNA expression of hHSC markers α-SMA and Cytoglobin B and v-ATPase subunits V1A, V1B2, V1C and v0c in hHSC treated with TGFβ1 and PDGF-BB for 24 hrs. (B) Representative western blot with histogram of v-ATPase subunits in hHSC treated with TGFβ1 and PDGF-BB for 24 hrs. Results are shown of 2 independent experiments obtained from 2 hHSC donors.

REFERENCES

1. Pinzani M. Pathophysiology of Liver Fibrosis. Dig Dis 2015;33:492-497.
2. Tsuchida T, Friedman SL. Mechanisms of hepatic stellate cell activation. Nat Rev Gastroenterol Hepatol 2017;14:397-411.
3. Di Sario A, Svegliati Baroni G, Bendia E, Ridolfi F, Saccomanno S, Ugili L, Trozzi L, et al. Intracellular pH regulation and Na+/H+ exchange activity in human hepatic stellate cells: effect of platelet-derived growth factor, insulin-like growth factor 1 and insulin. J Hepatol 2001;34:378-385.
4. Di Sario A, Baroni GS, Bendia E, D'Ambrosio L, Ridolfi F, Marileo JR, Jezequel AM, et al. Characterization of ion transport mechanisms regulating intracellular pH in hepatic stellate cells. Am J Physiol 1997;273:G39-48.
5. Nishi T, Forgac M. The vacuolar (H+)-ATPases--nature's most versatile proton pumps. Nat Rev Mol Cell Biol 2002;3:94-103.
6. Alzamora R, Al-Bataineh MM, Liu W, Gong F, Li H, Thali RF, Joho-Auchli Y, et al. AMP-activated protein kinase regulates the vacuolar H+-ATPase via direct phosphorylation of the A subunit (ATP6V1A) in the kidney. Am J Physiol Renal Physiol 2013;305:F943-956.
7. Gong F, Alzamora R, Smolak C, Li H, Naveed S, Neumann D, Hallows KR, et al. Vacuolar H+-ATPase apical accumulation in kidney intercalated cells is regulated by PKA and AMP-activated protein kinase. Am J Physiol Renal Physiol 2010;298:F1162-1169.
8. Kazgan N, Williams T, Forsberg LJ, Brenman JE. Identification of a nuclear export signal in the catalytic subunit of AMP-activated protein kinase. Mol Biol Cell 2010;21:3433-3442.
9. Ross FA, MacKintosh C, Hardie DG. AMP-activated protein kinase: a cellular energy sensor that comes in 12 flavours. FEBS J 2016;283:2987-3001.
10. Qiu SL, Xiao ZC, Piao CM, Xian YL, Jia LX, Qi YF, Han JH, et al. AMP-activated protein kinase alpha2 protects against liver injury from metastasized tumors via reduced glucose deprivation-induced oxidative stress. J Biol Chem 2014;289:9449-9459.
11. **Caligiuri A, Bertolani C**, Guerra CT, Aleffi S, Galastri S, Trappoliere M, Vizzutti F, et al. Adenosine monophosphate-activated protein kinase modulates the activated phenotype of hepatic stellate cells. Hepatology 2008;47:668-676.
12. Adachi M, Brenner DA. High molecular weight adiponectin inhibits proliferation of hepatic stellate cells via activation of adenosine monophosphate-activated protein kinase. Hepatology 2008;47:677-685.
13. Lim JY, Oh MA, Kim WH, Sohn HY, Park SI. AMP-activated protein kinase inhibits TGF-beta-induced fibrogenic responses of hepatic stellate cells by targeting transcriptional coactivator p300. J Cell Physiol 2012;227:1081-1089.
14. **Mederacke I, Dapito DH**, Affo S, Uchinami H, Schwabe RF. High-yield and high-purity isolation of hepatic stellate cells from normal and fibrotic mouse livers. Nat Protoc 2015;10:305-315.
15. **Rombouts K, Carloni V.** Determination and Characterization of Tetraspanin-Associated Phosphoinositide-4 Kinases in Primary and Neoplastic Liver Cells. Methods Mol Biol 2016;1376:203-212.
16. Longato L, Andreola F, Davies SS, Roberts JL, Fusai G, Pinzani M, Moore K, et al. Reactive gamma-ketoaldehydes as novel activators of hepatic stellate cells in vitro. Free Radic Biol Med 2017;102:162-173.
17. Rombouts K, Carloni V, Mello T, Omenetti S, Galastri S, Madiai S, Galli A, et al. Myristoylated Alanine-Rich protein Kinase C Substrate (MARCKS) expression modulates the metastatic phenotype in human and murine colon carcinoma in vitro and in vivo. Cancer Lett. 2013.
18. Rombouts K, Mello T, Liotta F, Galli A, Caligiuri A, Annunziato F, Pinzani M. MARCKS actin-binding capacity mediates actin filament assembly during mitosis in human hepatic stellate cells. Am.J.Physiol Cell Physiol 2012;303:C357-C367.

19. **Balasubramaniyan V, Dhar DK,** Warner AE, Vivien Li WY, Amiri AF, Bright B, Mookerjee RP, et al. Importance of Connexin-43 based gap junction in cirrhosis and acute-on-chronic liver failure. J Hepatol 2013;58:1194-1200.
20. Forgac M. Vacuolar ATPases: rotary proton pumps in physiology and pathophysiology. Nat Rev Mol Cell Biol 2007;8:917-929.
21. Crider BP, Xie XS, Stone DK. Bafilomycin inhibits proton flow through the H+ channel of vacuolar proton pumps. J Biol Chem 1994;269:17379-17381.
22. Kartner N, Yao Y, Li K, Crasto GJ, Datti A, Manolson MF. Inhibition of osteoclast bone resorption by disrupting vacuolar H+-ATPase a3-B2 subunit interaction. J Biol Chem 2010;285:37476-37490.
23. Vincent EE, Coelho PP, Blagih J, Griss T, Viollet B, Jones RG. Differential effects of AMPK agonists on cell growth and metabolism. Oncogene 2015;34:3627-3639.
24. Zhang LN, Xu L, Zhou HY, Wu LY, Li YY, Pang T, Xia CM, et al. Novel small-molecule AMP-activated protein kinase allosteric activator with beneficial effects in db/db mice. PLoS One 2013;8:e72092.
25. Xie XS, Padron D, Liao X, Wang J, Roth MG, De Brabander JK. Salicylihalamide A inhibits the V0 sector of the V-ATPase through a mechanism distinct from bafilomycin A1. J Biol Chem 2004;279:19755-19763.
26. Hawley SA, Fullerton MD, Ross FA, Schertzer JD, Chevtzoff C, Walker KJ, Peggie MW, et al. The ancient drug salicylate directly activates AMP-activated protein kinase. Science 2012;336:918-922.
27. Trautwein C, Friedman SL, Schuppan D, Pinzani M. Hepatic fibrosis: Concept to treatment. J Hepatol 2015;62:S15-24.
28. Koyama Y, Xu J, Liu X, Brenner DA. New Developments on the Treatment of Liver Fibrosis. Dig Dis 2016;34:589-596.
29. Rosenbloom J, Mendoza FA, Jimenez SA. Strategies for anti-fibrotic therapies. Biochim Biophys Acta 2013;1832:1088-1103.
30. Kawasaki-Nishi S, Nishi T, Forgac M. Proton translocation driven by ATP hydrolysis in V-ATPases. FEBS Lett 2003;545:76-85.
31. Stransky LA, Forgac M. Amino Acid Availability Modulates Vacuolar H+-ATPase Assembly. J Biol Chem 2015;290:27360-27369.
32. **Thoen LF, Guimaraes EL,** Dolle L, Mannaerts I, Najimi M, Sokal E, van Grunsven LA. A role for autophagy during hepatic stellate cell activation. J Hepatol 2011;55:1353-1360.
33. **Wu FR, Pan CX,** Rong C, Xia Q, Yuan FL, Tang J, Wang XY, et al. Inhibition of acid-sensing ion channel 1a in hepatic stellate cells attenuates PDGF-induced activation of HSCs through MAPK pathway. Mol Cell Biochem 2014;395:199-209.
34. Lalo U, Pankratov Y, North RA, Verkhratsky A. Spontaneous autocrine release of protons activates ASIC-mediated currents in HEK293 cells. J Cell Physiol 2007;212:473-480.
35. Dou C, Liu Z, Tu K, Zhang H, Chen C, Yaqoob U, Wang Y, et al. P300 Acetyltransferase Mediates Stiffness-Induced Activation of Hepatic Stellate Cells Into Tumor-promoting Myofibroblasts. Gastroenterology 2018.

Figure 1

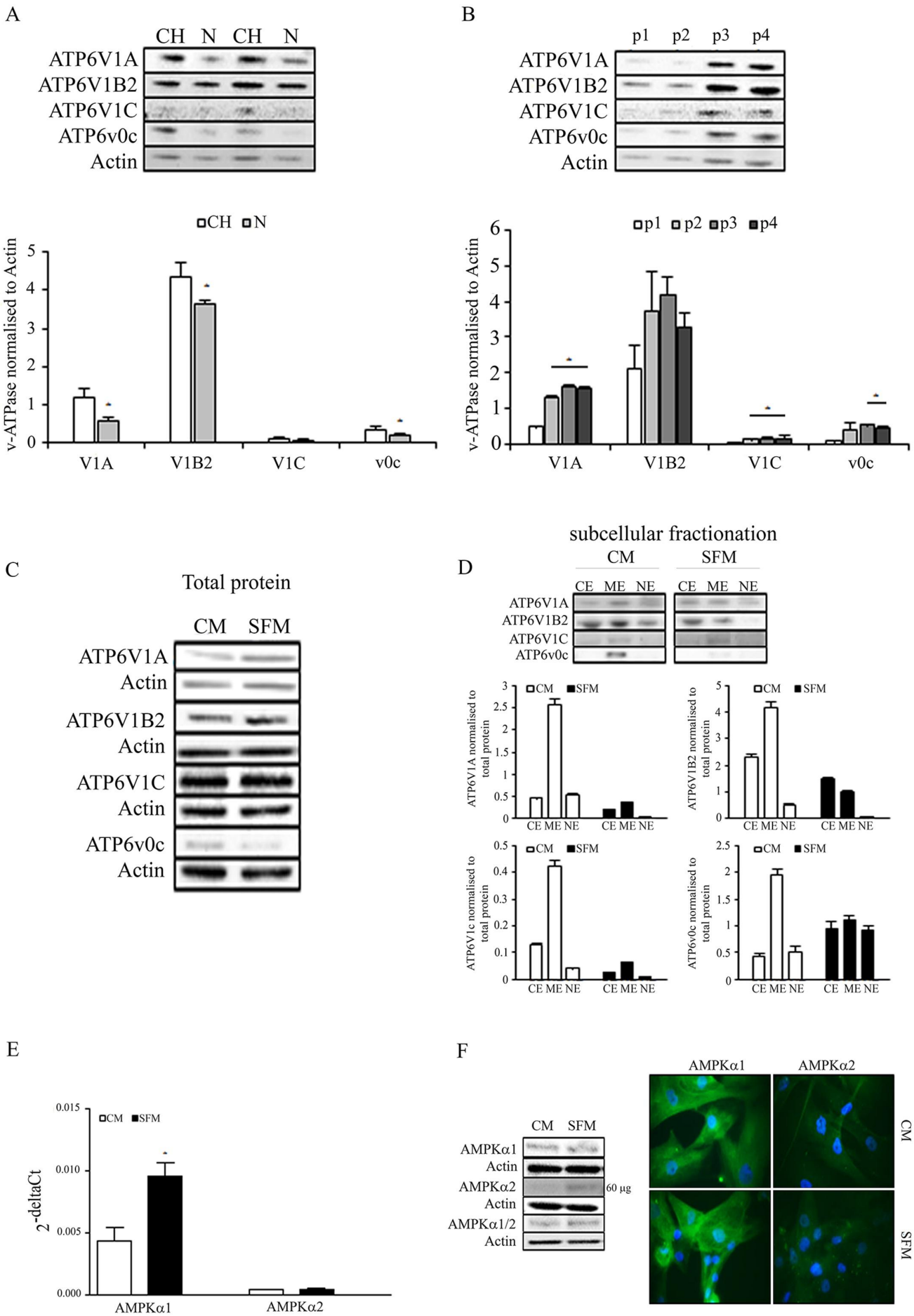
A
CH N CH N
ATP6V1A
ATP6V1B2
ATP6V1C
ATP6v0c
Actin
CH N
v-ATPase normalised to Actin
V1A V1B2 V1C v0c
B
p1 p2 p3 p4
ATP6V1A
ATP6V1B2
ATP6V1C
ATP6v0c
Actin
p1 p2 p3 p4
v-ATPase normalised to Actin
V1A V1B2 V1C v0c
C
Total protein
CM SFM
ATP6V1A
Actin
ATP6V1B2
Actin
ATP6V1C
Actin
ATP6v0c
Actin
D
subcellular fractionation
CM SFM
CE ME NE CE ME NE
ATP6V1A
ATP6V1B2
ATP6V1C
ATP6v0c
CM SFM
ATP6V1A normalised to total protein
ATP6V1B2 normalised to total protein
ATP6V1c normalised to total protein
ATP6v0c normalised to total protein
CE ME NE CE ME NE
E
CM SFM
2-deltaCt
AMPKα1 AMPKα2
F
AMPKα1 AMPKα2
CM SFM
AMPKα1
Actin
AMPKα2
Actin
AMPKα1/2
Actin
60 µg
CM
SFM

Figure 2

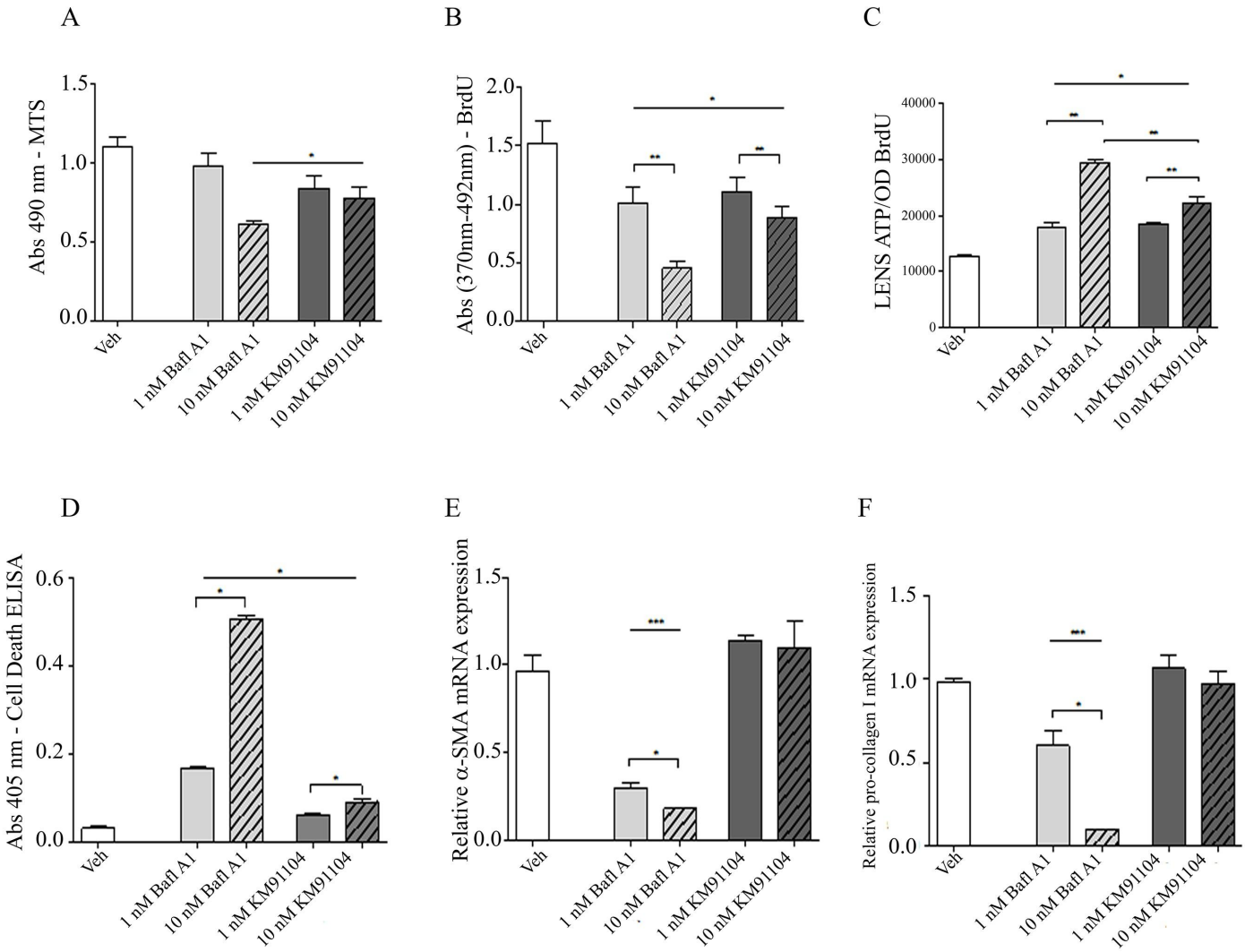
A
Abs 490 nm - MTS
1.5
1.0
0.5
0.0
Veh
1 nM Bafl A1
10 nM Bafl A1
1 nM KM91104
10 nM KM91104
B
Abs (370nm-492nm) - BrdU
2.0
1.5
1.0
0.5
0.0
C
LENS ATP/OD BrdU
40000
30000
20000
10000
0
D
Abs 405 nm - Cell Death ELISA
0.6
0.4
0.2
0.0
E
Relative α-SMA mRNA expression
F
Relative pro-collagen I mRNA expression

Figure 3

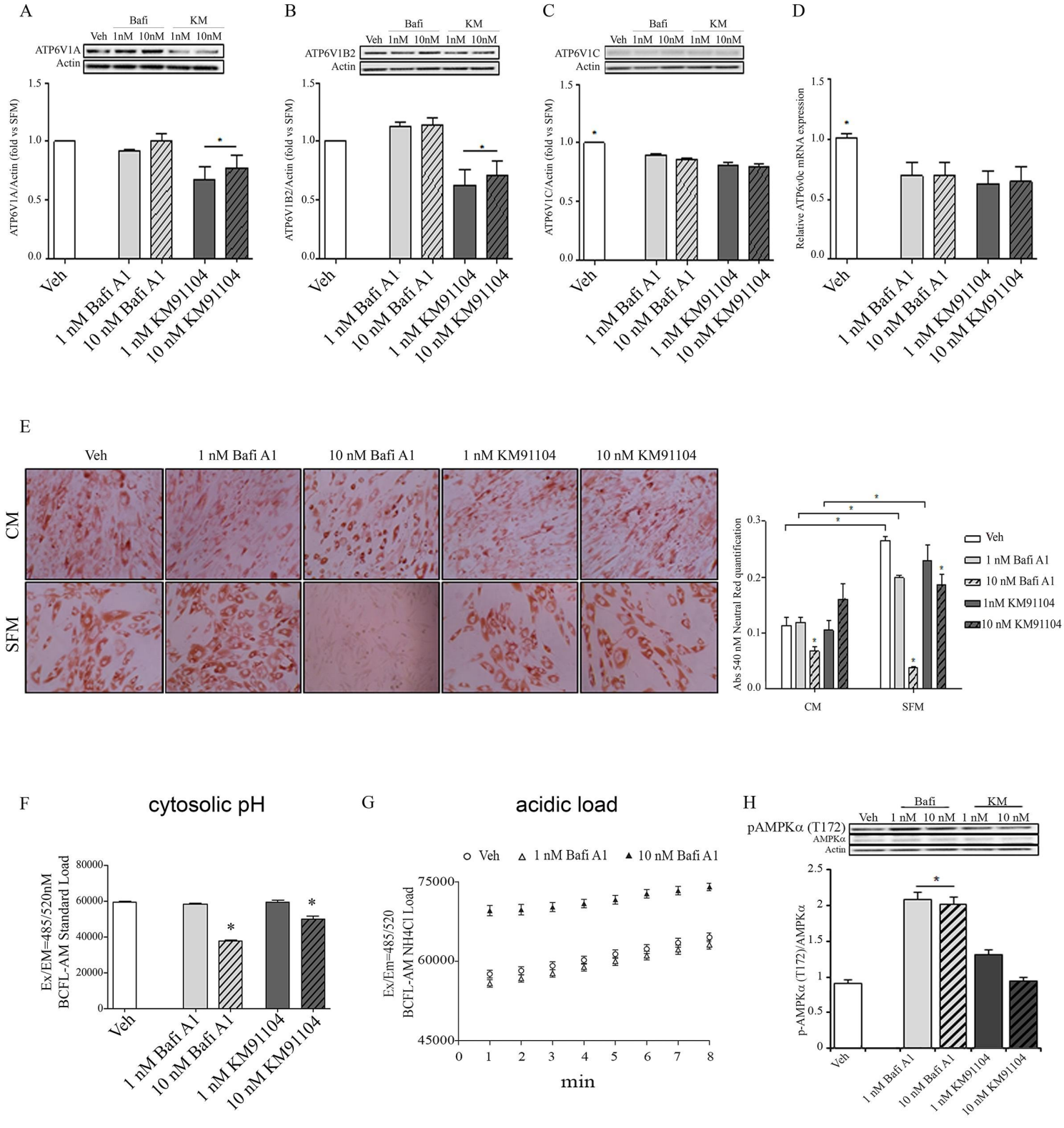
A
Bafi
KM
Veh 1nM 10nM 1nM 10nM
ATP6V1A
Actin
ATP6V1A/Actin (fold vs SFM)
B
ATP6V1B2
Actin
ATP6V1B2/Actin (fold vs SFM)
C
ATP6V1C
Actin
ATP6V1C/Actin (fold vs SFM)
D
Relative ATP6v0c mRNA expression
Veh
1 nM Bafi A1
10 nM Bafi A1
1 nM KM91104
10 nM KM91104
E
Veh
1 nM Bafi A1
10 nM Bafi A1
1 nM KM91104
10 nM KM91104
CM
SFM
Abs 540 nM Neutral Red quantification
F
cytosolic pH
Ex/EM=485/520nM
BCFL-AM Standard Load
G
acidic load
Veh
1 nM Bafi A1
10 nM Bafi A1
Ex/Em=485/520
BCFL-AM NH4Cl Load
min
H
pAMPKα (T172)
AMPKα
Actin
p-AMPKα (T172)/AMPKα

Figure 4

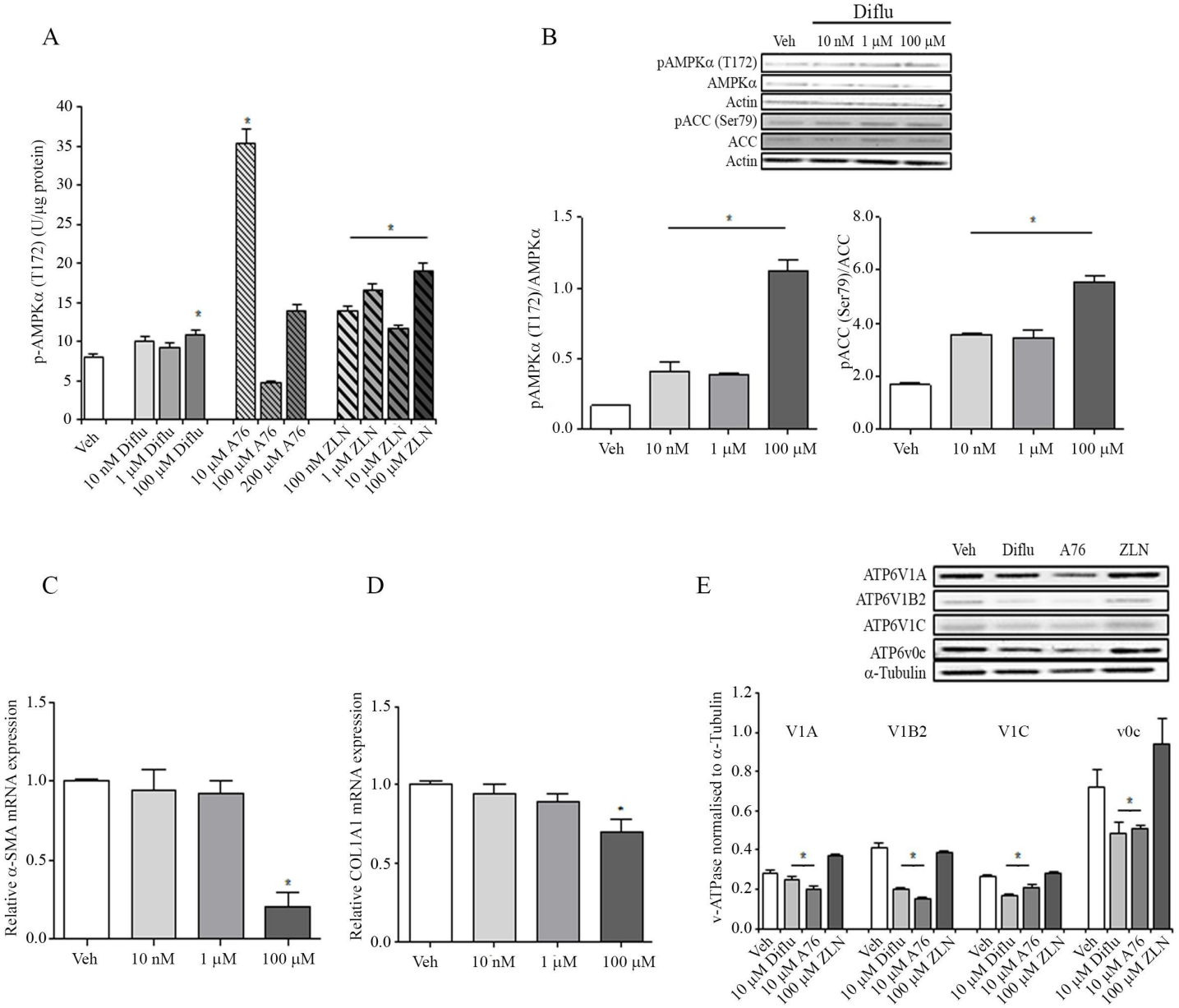
A
p-AMPKα (T172) (U/μg protein)
Veh
10 nM Diflu
1 μM Diflu
100 μM Diflu
10 μM A76
100 μM A76
200 μM A76
100 nM ZLN
1 μM ZLN
10 μM ZLN
100 μM ZLN
B
Diflu
Veh
10 nM
1 μM
100 μM
pAMPKα (T172)
AMPKα
Actin
pACC (Ser79)
ACC
Actin
pAMPKα (T172)/AMPKα
pACC (Ser79)/ACC
C
Relative α-SMA mRNA expression
D
Relative COL1A1 mRNA expression
E
Veh
Diflu
A76
ZLN
ATP6V1A
ATP6V1B2
ATP6V1C
ATP6v0c
α-Tubulin
v-ATPase normalised to α-Tubulin
V1A
V1B2
V1C
v0c

Figure 5

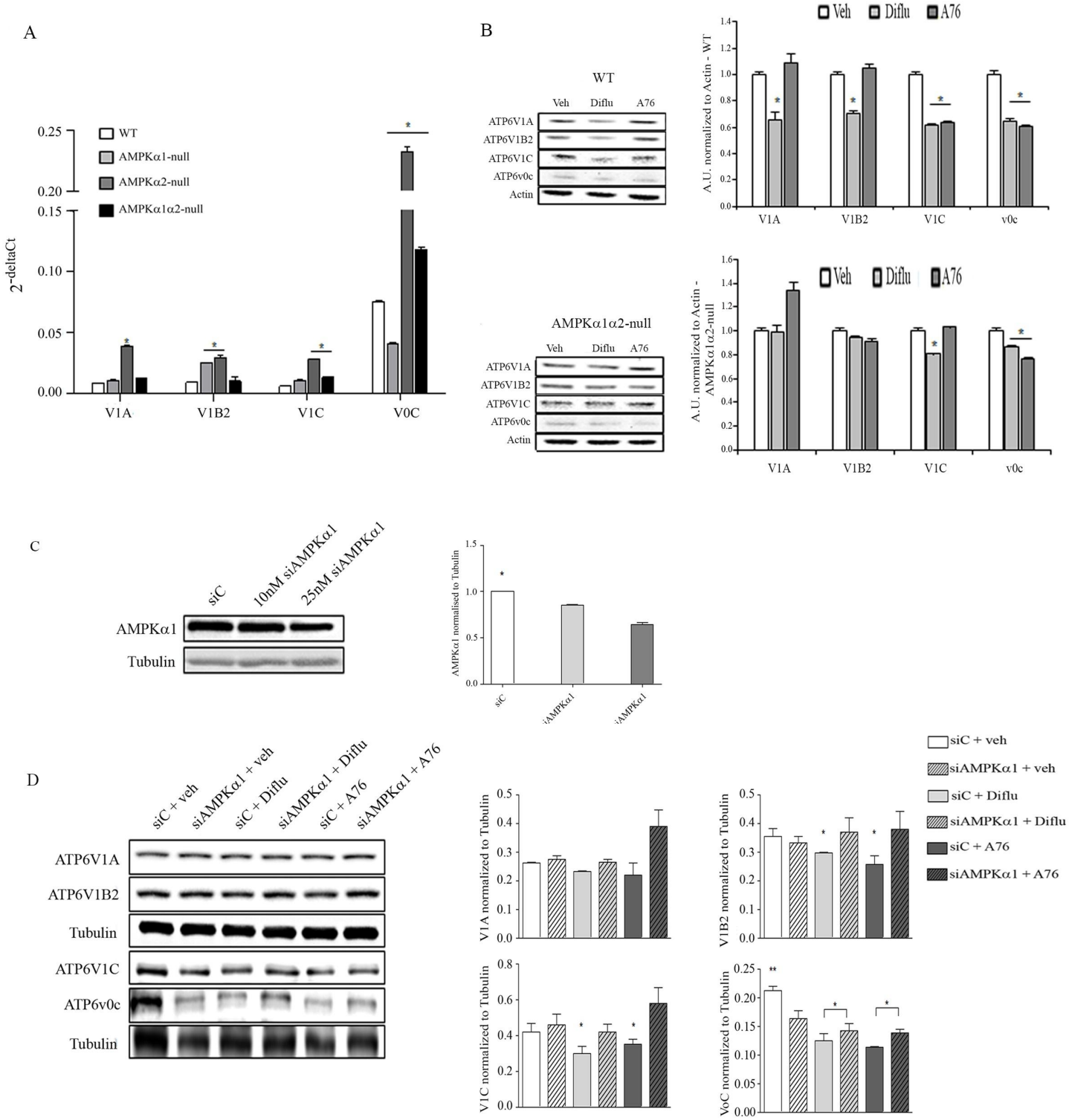
A
WT
AMPKα1-null
AMPKα2-null
AMPKα1α2-null
2-deltaCt
V1A
V1B2
V1C
V0C
B
WT
Veh
Diflu
A76
ATP6V1A
ATP6V1B2
ATP6V1C
ATP6v0c
Actin
A.U. normalized to Actin - WT
AMPKα1α2-null
A.U. normalized to Actin - AMPKα1α2-null
C
siC
10nM siAMPKα1
25nM siAMPKα1
AMPKα1
Tubulin
AMPKα1 normalised to Tubulin
D
siC + veh
siAMPKα1 + veh
siC + Diflu
siAMPKα1 + Diflu
siC + A76
siAMPKα1 + A76
ATP6V1A
ATP6V1B2
Tubulin
ATP6V1C
ATP6v0c
Tubulin
V1A normalized to Tubulin
V1B2 normalized to Tubulin
V1C normalized to Tubulin
VoC normalized to Tubulin

Figure 6

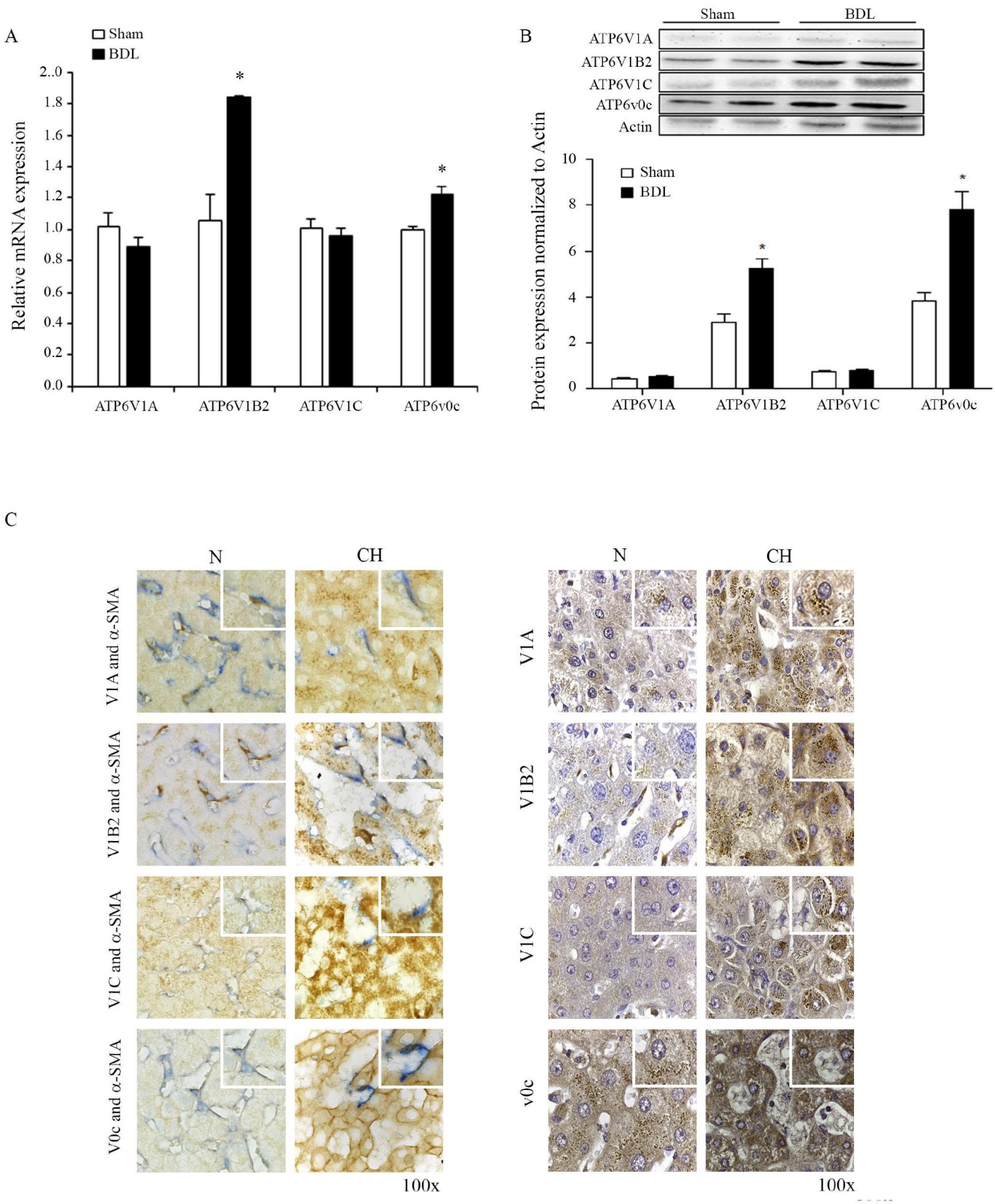
A
Sham
BDL
Relative mRNA expression
2..0
1.8
1.6
1.4
1.2
1.0
0.8
0.6
0.4
0.2
0.0
*
*
ATP6V1A
ATP6V1B2
ATP6V1C
ATP6v0c
B
Sham
BDL
ATP6V1A
ATP6V1B2
ATP6V1C
ATP6v0c
Actin
Protein expression normalized to Actin
10
8
6
4
2
0
Sham
BDL
*
*
ATP6V1A
ATP6V1B2
ATP6V1C
ATP6v0c
C
N
CH
V1A and α-SMA
V1B2 and α-SMA
V1C and α-SMA
V0c and α-SMA
100x
N
CH
V1A
V1B2
V1C
v0c
100x

Figure 7

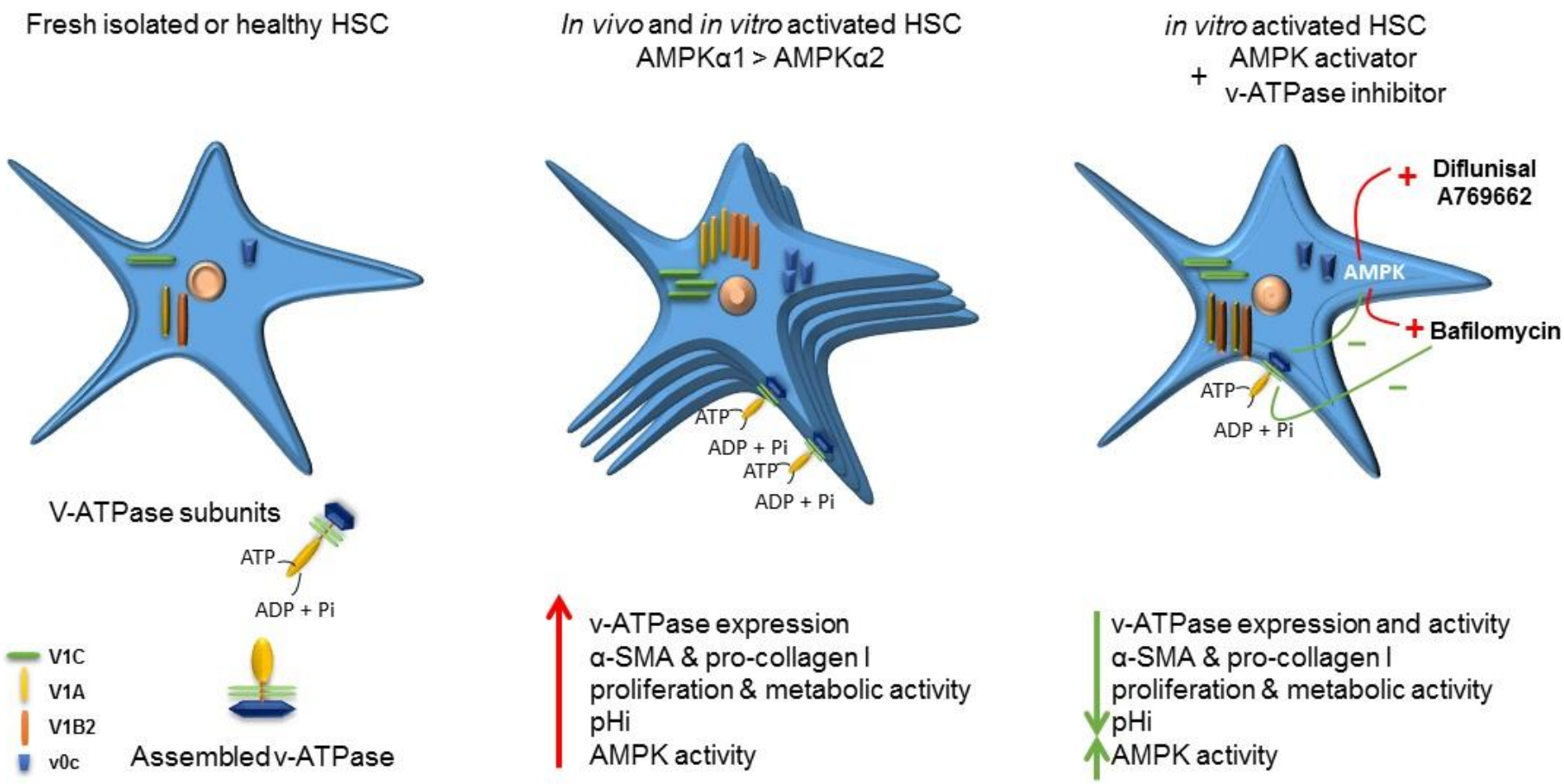
Fresh isolated or healthy HSC
In vivo and in vitro activated HSC
AMPKα1 > AMPKα2
in vitro activated HSC
+ AMPK activator
v-ATPase inhibitor
Diflunisal
A769662
AMPK
Bafilomycin
ATP
ADP + Pi
ATP
ADP + Pi
V-ATPase subunits
ATP
ADP + Pi
V1C
V1A
V1B2
v0c
Assembled v-ATPase
v-ATPase expression
α-SMA & pro-collagen I
proliferation & metabolic activity
pHi
AMPK activity
v-ATPase expression and activity
α-SMA & pro-collagen I
proliferation & metabolic activity
pHi
AMPK activity

Suppl. Figure 1

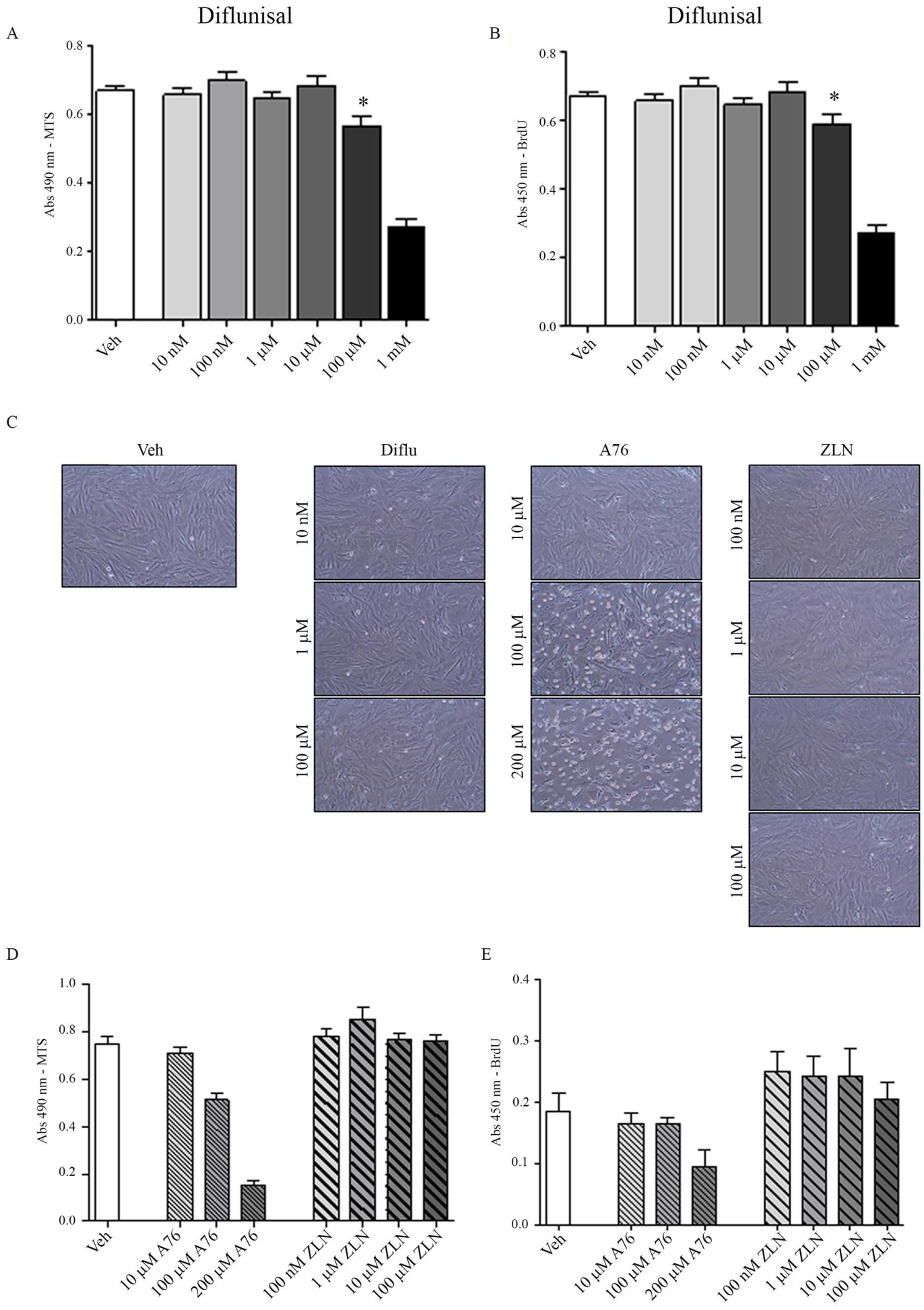

Supplementary Figure 2

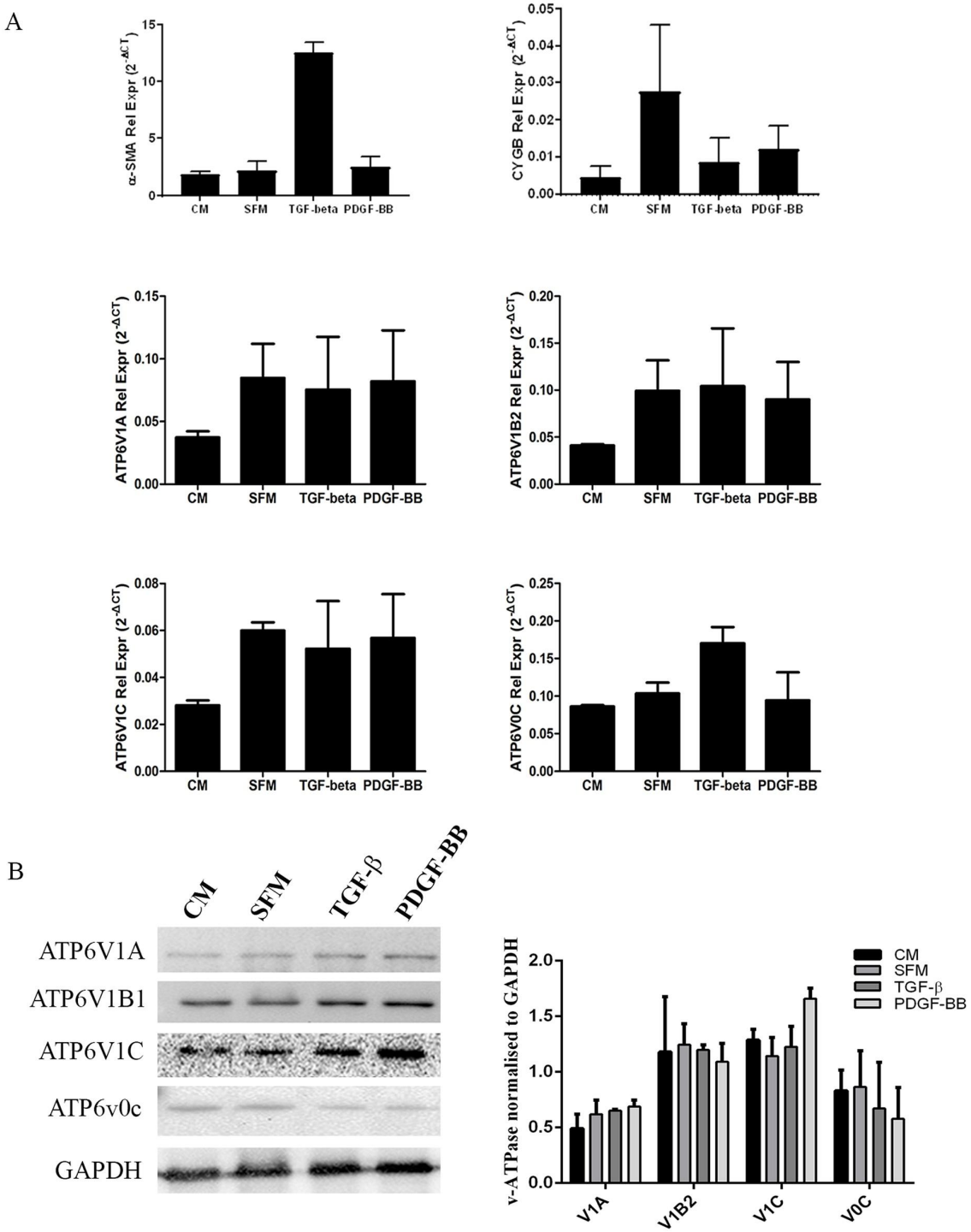

The AMPK-v-ATPase-pH axis: a key regulator of the pro-fibrogenic phenotype of human hepatic stellate cells.

Giusi Marrone[1], Francesco De Chiara[2], Katrin Böttcher[1], Ana Levi[1], Dipok Dhar[1], Lisa Longato[1], Giuseppe Mazza[1], Zhenzhen Zhang[1], Martina Marrali[1], Anabel Fernández-Iglesias[3], Andrew Hall[7], Tu Vinh Luong[7], Benoit Viollet[4,5,6], Massimo Pinzani[1], Krista Rombouts[1]

1. Regenerative Medicine & Fibrosis Group, Institute for Liver & Digestive Health, University College London, Royal Free Hospital, London, UK
2. Liver Failure Group, Institute for Liver & Digestive Health, University College of London, Royal Free Hospital, London, UK
3. Liver Vascular Biology Research Group, Barcelona Hepatic Hemodynamic Laboratory, IDIBAPS Biomedical Research Institute – CIBEREHD, Barcelona, Spain
4. INSERM, Institut Cochin, Paris, France
5. CNRS UMR 8104, Paris, France
6. Université Paris Descartes, Sorbonne Paris cité, Paris, France
7. Royal Free Hospital, Department of Cellular Pathology, London, UK

SUPPLEMENTARY MATERIALS AND METHODS

Human tissue samples

Normal (N) fresh human liver biopsies were obtained from 4 remnants from partial hepatectomy, and human cirrhotic biopsies were obtained from 4 remnants livers (alcoholic aetiology) obtained after transplantation (supplementary table 3) at Hospital Clínic of Barcelona. In all cases, one portion of fresh biopsies was fixed in

10% formalin and paraffin-embedded for the immunohistochemical analysis of V-ATPase subunits. Another portion of each normal and cirrhotic human liver tissue was used for HSC isolation. After isolation, one fraction of isolated HSC was pelleted and stored without culturing in standard 2D conditions and was marked as freshly isolated HSC passage 0, whereas another fraction of isolated cells (same donor) was cultured and subsequent passaged i.e. cultures from p1 to p4 which allows to investigate the HSC in vitro activation. Briefly, 20 g of human liver were perfused and digested with 0.01% DNase I and 0.01% collagenase for normal human liver or 0.014% collagenase for cirrhotic human liver. The homogenate was filtered through a 100µm cell strainer and the flow-through was centrifuged at 50xg for 5 minutes at 4°C. After washing the supernatant, gradient centrifugation was performed at 1400xg for 21 minutes at 4°C using an 11.5% Optiprep gradient. Finally, the interface was collected and washed (1). The Ethics committee of the Hospital Clinic de Barcelona approved the experimental protocol. Each patient signed the informed consent form (HCB/2015/0624).

Measurement of pHi and pHe

Relative intracellular pH changes were measured using the cell-permeable fluorescent indicator BCFL-AM. Cells were seeded and cultured overnight in complete medium at 30000 cells/well in a 96-well plate, followed by 24h in serum free medium. Next, cells were treated with the v-ATPase inhibitors for 48h. For the standard protocol, a dye loading solution was used according to the manufacturer's instruction (Sigma), adding 2mM probenecid, a non-specific inhibitor of anion exchange transporters. Cells were incubated, protected from light, in a 5% CO2, 37 °C incubator for 30 minutes and the pH assay was ran by measuring the

fluorescence at λex=485/λem=520 nm (FluoOmega spectrophotometer). For the acid load procedure, 5uL of freshly prepared 220 mM NH4Cl was added to each well and further incubated for 15 minutes at room temperature. Data were collected each minute for a total of 8 minutes by measuring the fluorescence at λex=485/λem=520 nm. For the pHe analysis, media was collected from hHSC cultured in SFM for 24h and after 24h-48h, depending on the treatment, prior to the measurement of the hydrogen-ion concentration with the pH meter. The investigator performing the measurement was not aware of the treatment.

Immunohistochemistry

v-ATPase subunit detection: Immunostaining of v-ATPase subunits was performed in paraffin-embedded liver sections from control and cirrhotic human livers. Liver sections were de-paraffinize and hydrate through xylenes (2x, 10 min each) and ethanol (1x, 5 min 100%, 95%, 90%, 70%, 50%). Sections were microwaved (640 W) for 10 minutes in 1L of antigen unmasking solution, citric acid base (Vector), and soaked in TBS with 0.04% Tween-20 (Sigma) for 5 minutes. The slides were then blocked in peroxidase (0.3% H_2O_2 in methanol) for 5 minutes, washed in TBS for 5 minutes, blocked in 2.5% normal horse serum (Vector) for 10 minutes and then incubated over night with primary antibodies for ATP6V1A, V1B2, V1C, v0c, all diluted 1:150 (supplementary table 4). The slides where incubated with a biotinylated universal pan-specific secondary antibody and diaminobenzidine used as chromogen (both from Vector). The omission of the primary antibody was used as negative control. All sections were dehydrated, cleared in xylene, mounted with DPX (Leica biosystems), cover slipped and observed using a Zeiss Axioskop 40. Images were captured with an Axiocam IcC5 using Zeiss Axiovision (version 4.8.2).

Double immunohistochemistry for V-ATPase subunit(s) and α-SMA:

Cases of both NASH and normal tissue were identified from the Royal Free hospital Archives between 2000 and 2014. To exclude other known aetiologies we conducted and both clinical and histology review of material.

To show the co- localisation of the ATP6V components with hepatic stellate cells the expression of ATP6V1A, ATP6V1B2, ATP6V0c and ATP6V1C was demonstrated in a double immunostain with αSMA. The antibodies used are described in Table 4 Supplementary Tables. Prior to the double immunostaining all antibodies were first optimised with positive controls and the following conditions were identified.

For ATP6V1A antigen retrieval was achieved by microwaving at 700W for 15 mins in 1L of pH 6.0 sodium citrate buffer, 10 mins for ATP6V1C and 20 mins for both ATP6V1B2 and ATP6V0c. Antigen retrieval for αSMA was performed by microwaving for 20 mins in 1L of pH 9.0 10mM Tris, 1mM EDTA buffer. Primary antibody dilutions are as follows ATP6V1A 1:50, ATP6V1B2 1:200, ATP6V0c 1:500 and ATP6V1C 1:200 and αSMA 1:500. The antibody binding of the ATP6V components were detected and visualised with the Novolink TM max polymer detection system kit (Novocastra) and the αSMA with Vector ImmPRESS™-AP Anti-Mouse Polymer Detection Kit (Vector Laboratories) and Vector Blue Alkaline Phosphatase substrate kit (Vector Laboratories).

The protocol is as follows: sections were dewaxed in xylene and taken to water through graded IDA (industrial denatured alcohol). Antigen retrieval was performed as specified above for each of the ATP6V components then the slides were then soaked in wash buffer for 5 mins, TBS with 0.04% Tween-20, slides were then blocked in the peroxidase blocking solution for 5 minutes and washed for a further 5

mins in the wash buffer. The slides were blocked for non-specific binding of the post primary using the Novolink protein block for 5 mins and then incubated in each of the ATP6V primary antibody for 1 hour. The slides were then placed for 30 minutes in the post-primary solution, 30 mins in the polymer solution and developed for 5 mins with 3,3′ di-amino-benzidine with a 5 minute buffer wash between each of the steps. On these same slides we then performed further antigen retrieval for the αSMA as detailed above (microwave 20 mins pH 9.0 Tris EDTA). The slides were blocked for non-specific binding of the ImmPRESS™ AP reagent using the R.T.U Normal horse Serum from the kit for 5 mins and then incubated in αSMA primary antibody for 1 hour. The slides were then placed for 30 minutes in the ImmPRESS™ AP and developed for 10 mins in Vector Blue substrate kit with a 5 minute buffer wash between each of the steps. The slides were washed in tap water and airdried before mounting. The slides were observed using a Zeiss Axioskop 40 (Zeiss, Cambridge, UK) and images were captured with an Axiocam IcC5 using Zeiss Axiovision (version 4.8.2).

Isolation and culture of human hepatic stellate cells (hHSC), Royal Free Hospital, London, UK.

Ten grams of total human liver tissue was digested with 0.01% Collagenase, 0.05% Pronase, and 0.001% DNase I without perfusion. The homogenate was filtered through a 100 µm cell strainer (BD Falcon,Oxford, UK), and the flow-through was centrifuged at 50xg for 2 minutes at 4°C. After washing the supernatant, gradient centrifugation was performed at 1400xg for 17 minutes at 4°C using an 11.5% Optiprep gradient (Sigma). Finally, the interface was collected and washed. Purity of the obtained HSC was confirmed by detection of CD140b, CD29 and Cytoglobin B.

The obtained HSC were cultured in Iscove's Modified DMEM (IMDM), supplemented with 20% foetal bovine serum (FBS), 2 mM Glutamine, 1X nonessential amino acids, 1.0 mM sodium pyruvate, 1X antibiotic-antimycotic (all from Life Technologies, Paisley, UK), referred to as complete hHSC medium (CM) hereinafter. Each hHSC preparation was maintained under standard conditions in a humidified incubator under 5% CO_2 in air at 37°C. Experiments described in this study were performed with hHSC cultured in complete medium (CM) or serum free medium (SFM) of at least three cell preparations and three replicates, used between passage 4 and 8 (except for Figure 1A and 1B), thus *in vitro* activated hHSC (Rombouts et al., Lipid Signalling Protocols, 2015).

Mouse embryonic fibroblasts (MEF) cell culture

Mouse embryonic fibroblasts (MEF) deficient in the genes encoding AMPKα1 (AMPKα1-null) or AMPKα2 (AMPKα2-null) or both isoforms of AMPK (AMPKα1α2-null) and corresponding wild-type MEF were provided by Dr. Benoit Viollet and described previously (2) (3). Results were derived from at least three replicates per group.

Treatment

v-ATPase inhibitors: Bafilomycin A1 and KM91104

hHSC and MEF were treated with Bafilomycin A1 (Sigma, B1793) which inhibits specifically the v-ATPase proton pump (V-ATPase subunit ATP6V0C/V0), and KM91104 (Calbiochem) a non-macrolide small molecule which specifically targets the interaction between v-ATPase subunit a3 and subunit B2 at low concentrations of 1nM and 10nM for 48h. Dimethyl sulfoxide (DMSO) was used as vehicle.

AMPK activators: *A769662, ZLN024 hydrochloride and Diflunisal*

HSC were incubated for 24h with freshly prepared Diflunisal (Sigma, D3281), a salicylic acid derivative with analgesic and anti-inflammatory effects, which has shown to be a strong CBP/p300 inhibitor, at different concentrations (10nM, 100nM, 1μM, 10μM, 100μM and 1mM) or with its vehicle (DMSO), for proliferation and metabolic activity assays. Non-toxic concentrations of 10nM, 1uM and 100uM were used for protein and RNA analysis. Diflunisal was found to be an effective AMPK activator at 100uM, which is the dose used to treat AMPKα1α2-null and WT MEFs. In another set of experiments, hHSC were treated with AMPK allosteric, direct activators A769662 and ZLN024 both inhibiting dephosphorylation of p-AMPK. Activator A769662 (4) was used at 10uM, 100uM and 200uM, whereas ZLN024 hydrochloride (Zhang LN et al., PlosOne 2013) was used at 100nM, 1uM, 10uM and 100uM, and its vehicle DMSO, for 24h. Both activators are from TOCRIS Biosciences. AMPKα1α2-null and WT MEF were treated with 10uM of A76 for 24h. TGFβ1 and PDGF-BB treatment: cells were cultured in 12 well plates (100.000/well) or 6 well plates (300.000/well) in complete culture medium. After 24 hours, medium was removed and cells were cultured for 24 hours in serum-free medium followed by a treatment with TGFβ1 (5ng/ml) or PDGF-BB (10ng/ml) for 24 hours. RNA was extracted (12 wells) or protein cell lysate (6 wells) was isolated as previously described (5).

Quantitative measurement of HSC proliferation and metabolic activity

Cells were seeded at a density of 8000cells/well/100uL on 96-well plates and treated with Bafilomycin, KM, Diflunisal, A76 and ZLN or left untreated for the indicated

concentrations and time points. Cell proliferation and metabolic activity were assessed by 5-bromo-2-deoxyuridine (BrdU, Roche) and the tetrazolium compound [3-(4,5-dimethylthiazol-2-yl)-5-(3-carboxymethoxyphenyl)-2-(4-sulfophenyl)-2H-tetrazolium, inner salt, MTS] (CellTiter 96 AQ_{ueous} One Solution Cell Proliferation Assay, Promega), respectively, according to the manufacturer's protocol. In metabolically active cells, the MTS tetrazolium compound is reduced via NAD(P)H-dependent dehydrogenase enzymes to generate a coloured formazan product that is soluble in cell culture media.

Neutral Red Uptake Assay

Cells were seeded at a density of 8000cells/well/100uL on 96-well plates and treated with Bafilomycin and KM (1 nM, 10 nM). After 48h treatment with v-ATPase inhibitors, cells were incubated for 3h with a medium containing 40µg/ml of Neutral Red (Sigma), a supravital dye incorporated and bound in the acid compartment/lysosomes of viable cells as described by Repetto et al. (6), washed in 1x PBS and differences in Neutral Red staining/distribution were examined under a phase-contrast inverted microscope, followed by the quantification at 540nm using a FluoOmega spectrophotometer. Measurements were performed in quadruplicates for each experimental condition and absorbance values were corrected for background.

RNA isolation and Quantitative Real-Time PCR

Total RNA was extracted using Qiazol reagent and RNeasy Universal Mini Kit (Qiagen,Manchester, UK). One µg of total RNA was reverse transcribed with random primers and MultiScribe RT enzyme (Applied Biosystems, Paisley,UK). Taqman® gene expression assays were used to measure via qPCR the levels of the transcripts

for different v-ATPase and AMPK subunits, and for markers of fibrogenic activation (supplementary table 5). Signal was acquired with Applied Biosystems 7500 Fast Real-Time PCR System (ThermoFisher Scientific, Paisley, UK) and data were expressed as either $2^{-\Delta\Delta Ct}$ or $2^{-\Delta Ct}$. GAPDH or HPRT1 served as endogenous controls (5).

Western Blot

Cells were seeded at a density of 350000cells/well/3mL in 6-well plates and treated as described before. The cellular lysis were performed using either the cell extraction buffer (Invitrogen, FNN0011) containing 1mM PMSF and 1:100 protease inhibitor cocktail (Sigma) for whole protein extraction or the subcellular protein fractionation Kit (Thermo Scientific, 78840) for cytoplasmic, membrane and nuclear protein extraction. Proteins were quantified via micro bicinchoninic (MBCA) assay (Pierce, Rockford, IL, USA) and stored at -80°C for further analysis. Ten μg of protein extracts were separated by SDS-PAGE with 8-12% acrylamide gel and transferred to a PVDF membrane (Millipore, Bedford, USA). After blocking for 1 h with 5% bovine serum albumin (BSA), membranes were incubated overnight 4 °C under mild agitation with primary antibody solutions (5% BSA, TBS 1X and 0.1%Tween 20). Membranes were then washed with TBS 1X/0.1% Tween 20, followed by incubation with secondary HRP-conjugated antibody for 1h at room temperature. The complete list of antibodies used is provided in supplementary table 4. Protein immuno-reactivity was revealed with the ECL system (Thermo Scientific, Pierce), using a FluorChem M (Protein Simple, San Jose, USA), and quantitative densitometric values of all proteins were normalized to Actin or Tubulin (5).

AMPKα activity

Cells were seeded at a density of 350000cells/well/3mL onto 6-well culture plates and treated with different concentrations of AMPK activators for 24h in SFM. Incubation was stopped by cell lysis and AMPK activity was determined by AMPKα expression using Enzyme Linked-Immuno-Sorbent Assay (ELISA) kit (KHO0651, Invitrogen), according to the supplier's protocol. Absorbance was measured at 450 nm using a FluoOmega spectrophotometer and the concentration of phosphorylated AMPKα was calculated and normalized to the protein concentration of the lysates (units/µg protein).

siRNA experiments

hHSC were seeded at a density of 350000cells/well/3mL in 6-well plates and transfected with siRNA targeting different regions of the respective transcript human AMPKα1 (10nM-25 nM, s101 and s102, Life Technologies), or with a negative control siRNA (25 nM, Life Technologies) using TurboFectin 8.0 as transfection agent (OriGene) according to the manufacturer’s instructions. Twenty-four hours post-transfection, cells were treated for an additional 24h with either 100 µM Diflunisal, 10uM A76 or its vehicle. The efficiency of the siRNA experiments was further validated by analysing AMPKα1 protein levels via western blotting as described before (5, 7).

REFERENCES

1. **de Mesquita FC, Guixe-Muntet S, Fernandez-Iglesias A,** Maeso-Diaz R, Vila S, Hide D, Ortega-Ribera M, et al. Liraglutide improves liver microvascular dysfunction in cirrhosis: Evidence from translational studies. Sci Rep 2017;7:3255.
2. Laderoute KR, Amin K, Calaoagan JM, Knapp M, Le T, Orduna J, Foretz M, et al. 5'-AMP-activated protein kinase (AMPK) is induced by low-oxygen and glucose deprivation conditions found in solid-tumor microenvironments. Mol Cell Biol 2006;26:5336-5347.
3. Viollet B, Andreelli F, Jorgensen SB, Perrin C, Flamez D, Mu J, Wojtaszewski JF, et al. Physiological role of AMP-activated protein kinase (AMPK): insights from knockout mouse models. Biochem Soc Trans 2003;31:216-219.
4. **Cool B, Zinker B**, Chiou W, Kifle L, Cao N, Perham M, Dickinson R, et al. Identification and characterization of a small molecule AMPK activator that treats key components of type 2 diabetes and the metabolic syndrome. Cell Metab 2006;3:403-416.
5. Longato L, Andreola F, Davies SS, Roberts JL, Fusai G, Pinzani M, Moore K, et al. Reactive gamma-ketoaldehydes as novel activators of hepatic stellate cells in vitro. Free Radic Biol Med 2017;102:162-173.
6. Repetto G, del Peso A, Zurita JL. Neutral red uptake assay for the estimation of cell viability/cytotoxicity. Nat Protoc 2008;3:1125-1131.
7. Rombouts K, Mello T, Liotta F, Galli A, Caligiuri A, Annunziato F, Pinzani M. MARCKS actin-binding capacity mediates actin filament assembly during mitosis in human hepatic stellate cells. Am.J.Physiol Cell Physiol 2012;303:C357-C367.

Timing/Treatment	Veh	Bafi 10nM	KM91104 10nM
0h	7.743 ± 0.009	7.752 ± 0.002	7.764 ± 0.03
24h	7.596 ± 0.003	7.609 ± 0.007	7.600 ± 0.05
48h	7.563 ± 0.007	7.549 ± 0.006	7.531 ± 0.01

Table 1: pH measurements (extracellular pH) of serum free medium collected 24h before and every 24h (up to 48h) after treatments of in vitro activated human HSC with v-ATPase inhibitors indicated in the table.

Timing/Treatment	Veh	Diflunisal 100uM	A769662 10uM
0h	7.644 ± 0.01	7.593 ± 0.05	7.647 ± 0.03
24h	7.560 ± 0.05	7.550 ± 0.09	7.615 ± 0.01

Table 2: pH measurements (extracellular pH) of serum free medium collected 24h before and 24h after treatments of in vitro activated human HSC with the AMPK activators indicated in the table.

	Sample	Aetiology	Surgery	Gender	Age
Control	Human 8		Metastasis from colon carcinoma	Man	82
	Human 18		Metastasis from colon carcinoma	Man	64
	Human 19		Metastasis from colon carcinoma	Female	72
	Human 23		Metastasis from colon carcinoma	Female	60
Cirrhotic	Human 6 CH1	Alcohol	Transplantation	Female	56
	Human 16 CH2	Alcohol	Transplantation	Man	63
	Human 17 CH3	Alcohol	Transplantation	Man	48
	Human 25 CH4	Alcohol	Transplantation	Man	57

Table 3: Human tissue samples

Antibody	Cat No	Source
ATP6v0c	ab104374	Abcam
ATP6V1B2	14488 (D307Q)	Cell Signaling
V-ATPase C1	sc-21211 (N-20)	Santa Cruz Biotechnology
V-ATPaseV1C1	HPA023943	Atlas Antibodies
ATP6V1A	GTX110815	Genetex
AMPKα	2532	Cell Signaling
AMPKα1	2795	Cell Signaling
AMPKα2	2757 & sc-19131 (C-20)	Cell Signaling & Santa Cruz Biotechnology
pAMPKα (Thr172)	2535	Cell Signaling
ACC	PA5-17564	Thermo Fisher Scientific
pACC (Ser79)	PA5-17725	Thermo Fisher Scientific
Actin	sc-1616 (I-19)	Santa Cruz Biotechnology
ASMA	M085101-2	Agilent Dako
Tubulin	2144	Cell Signaling

Table 4: List of antibodies used in the study

Gene	Cat No	Source
GAPDH	Hs02758991_g1	Life Technologies LTD
HPRT1	Hs02800695_m1	Life Technologies LTD
ACTA2	Hs00426835_g1	Life Technologies LTD
COL1A1	Hs00164004_m1	Life Technologies LTD
AMPKα1	Hs01562315_m1	Life Technologies LTD
AMPKα2	Hs00178903_m1	Life Technologies LTD
ATP6v0c	Hs00798308_sH	Life Technologies LTD
GAPDH	Hs02758991_g1	Life Technologies LTD
HPRT1	Mm00446968_m1	Life Technologies LTD
ATP6V1C1	Mm01158129_m1	Life Technologies LTD
ATP6V1A	Mm00431979_m1	Life Technologies LTD
ATP6V1B2	Mm00431987_m1	Life Technologies LTD
ATP6v0c	Mm00821690_g1	Life Technologies LTD

Table 5: List of Taqman® assays used in the study